

UNIVERSITY OF OKLAHOMA

GRADUATE COLLEGE

ROLE OF METAL AND ACID CATALYTIC FUNCTIONS
IN THE LIQUID PHASE UPGRADING OF BIOMASS-DERIVED COMPOUNDS

A DISSERTATION

SUBMITTED TO THE GRADUATE FACULTY

in partial fulfillment of the requirements for the

Degree of

DOCTOR OF PHILOSOPHY

By

PURIDEJ WARAKUNWIT

Norman, Oklahoma

2018

ROLE OF METAL AND ACID CATALYTIC FUNCTIONS
IN THE LIQUID PHASE UPGRADING OF BIOMASS-DERIVED COMPOUNDS

A DISSERTATION APPROVED FOR THE
SCHOOL OF CHEMICAL, BIOLOGICAL AND MATERIALS ENGINEERING

BY

Dr. Daniel E. Resasco, Chair

Dr. Lance L. Lobban

Dr. Steven P. Crossley

Dr. Bin Wang

Dr. Laura E. Bartley

To my loving family.

ACKNOWLEDGMENTS

I am thankful to many wonderful people whom without them this dissertation would not be possible.

First and foremost, I would like to express the deepest gratitude to Professor Daniel E. Resasco, my advisor. It has been an honor for me to be part of his research team for the past five years, to experience his passion for catalysis research. Not only has he guided me through my dissertation but he has taught me to think and challenge myself. I must thank you for all your understanding, encouragement and support in these five years. Thank you for being a part of my Ph.D.'s chapter.

Secondly, I also owe a great gratitude to my undergraduate's advisor and also the person, who encourage me to study at graduate level, Dr. Tawan Sooknoi. I am grateful to Dr. Steven Crossley, Dr. Lance Lobban, Dr. Richard Mallinson and Dr. Jimmy Faria for their helpful criticism and discussion in the group meeting. I would like to thank Dr. Laura Bartley for being my committee member.

My appreciation to James Miles, Denis McAlister and all the staff at CBME office for their tremendous help that ensured smooth progress in my research.

I would like to thank every Biofuels member, both current and past, whom I have had a pleasure to meet and collaborate with. I enjoy the friendship I have made with Tu, Dachuan, Taiwo, Abhishek, Ali, Lu, Qiaohua, Gonghua, Karl, Danny, Felipe, Adam, Alex, Zheng, Tuong, Yen, Monica, Rajiv, Dixon, Camilla, and Cristiane. Special mention to Cristian and Nhung, words cannot describe how much I appreciate your companies. Thank you for all the laughs and memories you have shared with me in Norman.

I would especially like to thank all my Thai friends, Beam, Belle, Tam, P'Som, P'Pui, P'Mink, P'Ni, P'Kwang, P'Mot, P'Ple, P'Tuam, and P'Tink. I will always remember the memories we made in the USA.

I am most grateful to my wonderful family. I am blessed to have their support, understanding, and love in my life. Without them, I would not have gotten where I am today.

Finally, I would like to acknowledge the financial support for this research from Department of Energy.

TABLE OF CONTENTS

Acknowledgments.....	iv
List of Figures.....	ix
List of Tables.....	xii
Chapter 1. Introduction and Research Direction.....	1
Chapter 2. Ethanolysis of Lignin in High-Pressure Batch Reactor	3
2.1 Introduction.....	3
2.2 Experimental.....	9
2.2.1 Catalyst Synthesis	9
2.2.2 Lignin Characterization	9
2.2.3 Reaction Experiment and Product Characterizations	9
2.3 Results and Discussion	12
2.3.1 Lignin Depolymerization.....	12
2.3.2 Ethanol Conversion over Ru/SiO ₂	17
2.3.3 Carbon content in the catalyst after the reaction.....	21
2.3.4 NMR study on lignin	22
2.3.5 Red Oak Ethanolysis.....	28
2.3.6 Pyrolysis study of oak residue	32
2.4 Conclusions.....	36
Chapter 3. Hydrogenation of Diphenyl Ether over Ru/SiO ₂	38
3.1 Introduction.....	38
3.2 Experimental.....	40
3.2.1 Catalyst Synthesis and Characterization.....	40

3.2.2 Reaction Experiment.....	41
3.3 Results and Discussion	42
3.3.1 Catalyst Characterization.....	42
3.3.2 Catalytic Performance of Ru/SiO ₂	43
3.3.3 Bicyclic molecules formation	48
3.4 Conclusions.....	54
Chapter 4. C-O Bond Cleavage of Diphenyl Ether over PdOTS/HY.....	55
4.1 Introduction.....	55
4.2 Experiments	57
4.3 Results and Discussion	58
4.3.1 Role of Hydrophobicity	58
4.3.2 Role of metal and acid sites	61
4.3.3 C-O Cleavage.....	63
4.3.4 Kinetic fitting of hydrogenation of phenol and hydrogenation of cyclohexanone.....	67
4.3.5 Metals and Acid Sites Balance	69
4.4 Conclusions.....	70
Future Directions and Recommendations.....	71
References.....	73
Appendix A. Effect of External Water on Acetone Aldol Condensation over MgO.....	80
A1 Introduction.....	80
A2 Catalyst and Reaction Experiments	83
A2.1 Combusted MgO Preparation and Characterizations.....	83

A2.2 Reaction Experiments	84
A3 Results and Discussions	85
A4 Conclusion	91
Appendix B. Supplementary Figures and Tables	92

LIST OF FIGURES

Figure 2.1. HSQC-NMR spectra of lignin and prominent structures for identification from [9].	4
Figure 2.2. Quartz tube for pyroprobe pyrolysis.	11
Figure 2.3. Percentage of monomers yield from methanol and ethanol at 280°C, 1500 psi H ₂ and 12 hours.	14
Figure 2.4. Percentage of monomers yield from methanol with or without Ru/SiO ₂ at 280°C, 1500 psi H ₂ and 12 hours.	15
Figure 2.5. Percentage of monomers yield from ethanol with or without Ru/SiO ₂ at 280°C, 1500 psi H ₂ and 12 hours.	16
Figure 2.6. Selectivity from the conversion of ethanol over Ru/SiO ₂ (a) gas products selectivity and (b) liquid products selectivity.	18
Figure 2.7. 2D-HSQC of acetylated lignin sample.	23
Figure 2.8. 2D-HSQC NMR spectrum from (a) untreated lignin, (b) ethanol treatment and (c) ethanol treatment over Ru/C.	27
Figure 2.9. XRD of (a) raw oak, (b) ethanol treatment at 80°C and (c) ethanol treatment at 280°C.	30
Figure 2.10. SEM of raw oak (top left), ethanol treatment at 80°C (top right) and ethanol treatment at 280°C (bottom left and right).	31

Figure 2.11. Schematic of the breaking down of cellulose, hemicellulose, and lignin in red oak treating ethanol.....	32
Figure 2.12. Carbon yields from pyroprobe of residue from oak treatment in ethanol at 250°C and 280°C. Conditions: 520°C for 60 seconds.....	33
Figure 2.13. Carbon yields from pyroprobe of residue from oak treatment in ethanol at 280°C and Stage 3 torrefaction (520°C for 60 seconds).....	34
Figure 2.14. Liquid products from oak ethanolysis pyrolyzed at 520°C.....	35
Figure 2.15. Proposed process strategy of the ethanolysis from extracting biomass to non-pyrolytic bio-oil to the high-value chemicals upgrading.....	36
Figure 3.1. TPR of Ru/SiO ₂	42
Figure 3.2. FTIR of Ru/SiO ₂	43
Figure 3.3. Conversion of diphenyl ether over 5% Ru/SiO ₂ at a different time.....	45
Figure 3.4. Product Yield over different time.....	46
Figure 3.5. Conversion of diphenyl ether and products yield over a different amount of catalyst.....	47
Figure 3.6. Yield of products over Ru/TiO ₂ and Ru/SiO ₂	49
Figure 3.7. Reaction pathway of diphenyl ether over Ru/SiO ₂	50
Figure 3.8. Two possible rearrangement pathways to the C-C formation.....	52

Figure 3.9. Yield and selectivity of products over 5%PdOTS/HY.....	53
Figure 4.1. Mole of products over different mass of catalyst.....	60
Figure 4.2. Reaction pathways of rearrangement, alkylation of phenol and cyclohexene and alkylation of phenol and m-cresol.....	65
Figure 4.3. Reaction pathways of diphenyl ether over PdOTS/HY.....	69
Figure 4.4. Ratio of a total mole of C-C/Cyclohexane over different conversion.....	69
Figure A.1. Reaction pathway of acetone aldol condensation.....	81
Figure A.2. Rate of formation of 2-cyclopentylidene-cyclopentanone over different volume of external water on different MgO catalysts in organic phase reaction from Duong Ngo's research.....	83
Figure A.3. Total yield of products over MgO, MgO(80)-OTS(20) and MgO(80)- ETS(20) at 250°C.....	86
Figure A.4. Mechanism for mesityl oxide formation.....	88
Figure A.5. Mechanism for isophorone formation.....	89
Figure A.6. Influence of addition of water on aldol condensation activity over MgO, MgO(80)-OTS(20) and MgO(80)-ETS(20) at 250°C.....	90
Figure B.1. Chromatogram of lignin ethanolysis.....	94

LIST OF TABLES

Table 2.1. Summary of recent reports on monomer yields over various solvents and catalyst.	7
Table 2.2. Lignin Disappearance in methanol and ethanol solvent at different temperatures.	12
Table 2.3. Mole of products from the conversion of ethanol over (a) Ru/SiO ₂ , (b) Ru/SiO ₂ and lignin, (c) spent catalyst from reaction (b) and (d) without catalyst only lignin.	20
Table 2.4. Carbon content of lignin residues after ethanolysis.	21
Table 3.1. Conversion of diphenyl ether at different reaction temperatures. Reaction conditions: 0.15 M diphenyl ether, decalin (25 mL), 5 MPa H ₂ , 500 rpm.	44
Table 3.2. Yield of products over two different ruthenium precursor: RuCl ₃ and Ru(NO)(NO ₃) ₃	51
Table 4.1. Conversion and carbon balance of PdOTS/HY and Pd/HY in organic phase and biphasic system.	59
Table 4.2. Products yield and carbon balance of diphenyl ether reaction over OTS/HY, 2% Pd/SiO ₂ and 1% PdOTS/HY.	61
Table 4.3. Products yield and selectivity of diphenyl ether over Pd/SiO ₂ and PdOTS/HY	62

Table 4.4. Products yield and selectivity of cyclohexyl phenyl ether over PdOTS/HY.	64
Table 4.5. Molar ratio of C-C products from alkylation of m-cresol/C-C products from rearrangement or alkylation of phenol.....	66
Table 4.6. Products selectivity of alkylation m-cresol and cyclohexanone.....	66
Table 4.7. Rate constants of hydrogenation of phenol (k_1) and hydrogenation of cyclohexanone (k_2).....	67
Table B.1. Effective Carbon Number (ECN) contributing to each compound groups from [71].	92
Table B.2. Effective carbon number and respond factor for each monomers from lignin ethanolysis.....	93

ABSTRACT

With higher demanding of fossil fuels and the growing problems of the greenhouse effect and global warming, biofuels have drawn much attention in the research study to understand the chemistry and seek the solution to the challenges in the both in processing and economic. In this study, ethanolsis of lignin for the conversion to monomers were investigated. With the rich ether bond linkages in lignin and in order to understand more of a fundamental chemistry, 4-O-5 ether bond model compound was also studied over Ru/SiO₂ and PdOTS/HY.

In the first part, ethanolsis of stillage lignin from bioethanol plant was studied in a high-pressure reactor. Ethanol shows to be an excellent solvent and source of hydrogen donor to depolymerize lignin. Performing the depolymerization at 280°C in 1400 psi of H₂, lignin disappearance was accounted for 60%. When the reaction was conducted with the addition of Ru/SiO₂, up to 95% of solid lignin was solubilized. However, in any conditions, the maximum monomers yield was 8%. A thorough study has shown that at 280°C, ethanol converts to acetaldehyde, which condensates to longer chain molecules that could potentially be blocking the active site. The catalysts also contained up to 7% of coke, which could be preferentially from trapping of larger trimers and oligomers during lignin depolymerization.

The second part of the study employed the methodology from the lignin depolymerization to biomass deconstruction. Ethanol solubilized up to 58% of the solid Red Oak. However, less than 1% of monomers yield were detected. Upon thermal pyrolysis of the oak residue from the ethanolsis step, it suggests that most of hemicellulose and cellulose remained intact in the biomass after severe ethanolsis,

which is shown in a large number of sugars and furan derivatives detected. The ethanolysis has proved to be an excellent method to isolate lignin from biomass.

The third part of this research looks into understanding the chemistry to break 4-O-5 ether linkage by studying diphenyl ether over Ru/SiO₂ and PdOTS/HY. In the hydrogenation of Ru/SiO₂, a surprising result suggest a carbon-carbon bond formation from the catalyst that was synthesized from the ruthenium(III) chloride precursor. The acidity that catalyzed this reaction is the Lewis acid sites on the ruthenium ions in the form of RuCl₃. This ion salt came from an incomplete calcination of the precursor at 500°C. From these results, PdOTS/HY catalyst was developed to maximize the carbon-carbon molecules. Upon the investigation, it shows that the carbon-carbon bond formation is maximized by a well-balanced metal and acidity. The most favorable pathway to the carbon-carbon molecule is through a partial hydrogenation of diphenyl ether followed C-O bond cleavage then alkylation of phenol and cyclohexene.

Chapter 1. Introduction and Research Direction

Fossil fuels have been the primary source of energy to produce electricity and transportation fuels. In the past decades, alternative energy has been studied to produce clean and efficient energy to replace fossil fuels. Even though that the conventional fossil fuels have superior advantages over other alternative energy, but burning fossil fuels creates tons of carbon dioxide, one of the major causes of global warming and greenhouse effect. Besides carbon dioxide and other poisonous gases such as SO_x and NO_x , are causing acid rain that affects forests and lakes environment. Numerous researches highlight the advantages of alternative energy to replace the fossil fuels. One of the alternative energy that has gained tremendous attention is liquid fuels from the conversion of biomass.

Lignocellulosic biomass is composed of cellulose, hemicellulose, and lignin. Depending on the source of the biomass, the content of each component varies. Different strategies to upgrade the biomass to valuable biofuels and chemicals have been proposed. Pyrolysis of biomass yields viscous bio-oil that contains a mixture of hundreds of compounds. Bio-oil usually contains up to 20-40 wt.% of oxygen and highly functionalized molecules, which are significantly different from petroleum feedstock. Conventional strategy to increase the energy density of pyrolytic bio-oil is first deoxygenating to reduce the reactivity of the feedstock then selectively upgrade the platform molecules to other fuels and chemicals [1][2][3]. Pyrolysis of biomass can result in recalcitrant lignin meaning that aromatics polymer are more connected through carbon-

carbon bonds [4]. Transitioning from petroleum to biomass presents significant technological and economic challenges.

With many challenges to develop biomass-based process, catalysis will play an important role to advance the technology. This dissertation will present the strategies for the conversion of lignocellulosic biomass particularly lignin and biomass-derived molecules utilizing heterogeneous catalysts. Three research topics are covered

- (i) Ethanolysis of lignin in the high-pressure batch reactor,
- (ii) Liquid phase hydrogenation of diphenyl ether over Ru/SiO₂,
- (iii) Liquid phase C-O bond cleavage of diphenyl ether over PdOTS/HY.

In each part, a literature review is followed by detailed experimental information with results and discussion of the topics.

Chapter 2. Ethanolysis of Lignin in High-Pressure Batch Reactor

2.1 Introduction

Lignocellulosic biomass, which composes of cellulose, hemicellulose, and lignin, is an abundant and renewable resource. For many decades, researchers have studied this complex structure from the formation to the depolymerization. The transformation of these constituents can offer broad varieties of bio-derived fuels and chemicals [5][6][7].

Lignin is a complex polymer deriving from methoxylated hydroxycinnamyl alcohol building blocks. Lignin is linked by different bonding which demand different conditions for cleavage. Owing to its high carbon-to-oxygen content, lignin has a great potential for biofuel feedstocks. Arrays of depolymerization conditions have been reported both “mild” and “harsh” conditions. Characterization of lignin components requires the use of a broad array of techniques. The chemical composition of the volatile liquid products is most often performed in Gas Chromatography-Mass Spectrometry (GC-MS) and Gas Chromatography-Flame Ionization Detector (GC-FID). However, there are always limitations to both identification and quantification as the original samples are not commercially available for many of the products. Lignin oil usually contains non-volatile and higher-molecular-weight molecules which are not detectable by GC-MS and GC-FID. Therefore, the employment of Gel Permeation Chromatography (GPC) will approximate the molecular weight and size distribution. With an advance in the technology of NMR, it has been widely used to reveal the linkages. Heteronuclear Single-Quantum Coherence (HSQC) experiment has been taken over from the simple tradition 1D-NMR. The experiment allows cross-coupling of the signals and provides higher

resolution to distinguish the structural details [6]–[8]. An example of 2D HSQC of lignin and the labeling is shown in Figure 2.1

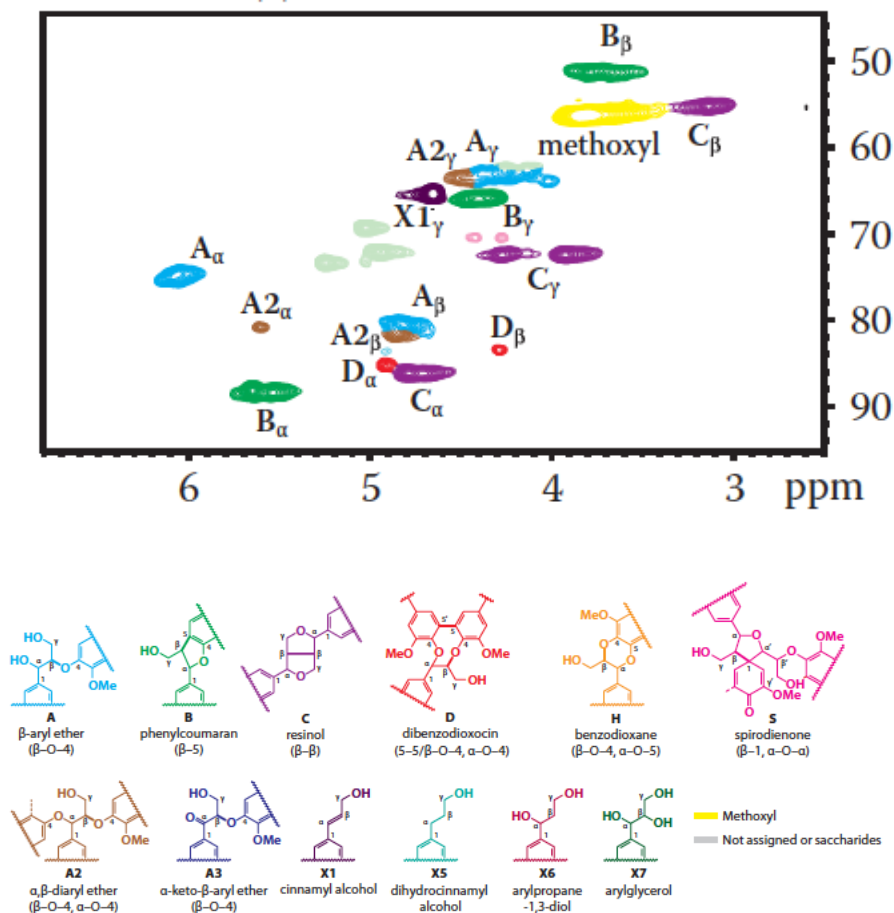


Figure 2.1. HSQC-NMR spectra of lignin and prominent structures for identification from [9].

Native lignin structure may suffer severe transformation from the pulping or pretreatment process depending on the temperature and duration of the process. Therefore, the abundance of each linkage motif is likely to differ from the native lignin. Two specific pulping processes that are widely used are Kraft and Organosolv processing. Kraft process is the main technology in the paper industry. The process involves treating the woods with hot water, sodium hydroxide, and sodium sulfide at 170°C to 176°C for

several hours. During the process, the liquor is maintained at pH value > 10 to avoid the re-deposition of lignin residues onto the fibers [10]. During the delignification steps, the contents of β -o-4 and other β -ether have significantly decreased. Lignin network becomes recalcitrant, meaning that the network comes to be highly condensed and formed C-C crossed link [11].

Acidolysis of β -ethers in lignin was studied to understand the rate of phenolic/non-phenolic β -ethers hydrolysis. Sturgeon et al. observed that hydrolysis of phenolic model compounds was about two orders of magnitude faster than for non-phenolic counterparts with H_2SO_4 at 150°C . This study suggests the importance of selecting the model compounds regarding the linkages cleavage [12].

One of the disadvantages of Kraft lignin is the emission of sulfur compounds such as hydrogen sulfide, methyl mercaptan, and dimethyl sulfide. Organosolv lignin has been highlighted as an alternative to Kraft process. Pulping entails organic solvent treatment such as aqueous ethanol. It was demonstrated to release fraction of lignin and hemicelluloses into the solution. Different alcohols from methanol to isopropanol have been proven to be able to dissolve the biomass [4][13][14]. Moreover, the Organosolv process allows the recovery of the solvent, unlike the Kraft process.

Isolating sugars from biomass was reported using γ -valerolactone (GVL) without ionic liquids or concentrated acids. At the same time lignin depolymerized and isolated separately. The lignin structure was maintained after the extraction as confirmed by their NMR study of before and after the treatment. Isolated lignin was upgraded using two-stage hydrolysis. First, the lignin was dissolved in 80% THF, 8.5% H_3PO_4 , and 1.5% H_2O

over Ru/C at 150°C. Then, THF solvent was replaced with heptane forming a biphasic mixture that then was treated at 250°C. Up to 38% of soluble lignin-derived monomers was observed [15].

Whether or not lignin undergoes recondensation also depends on the choice of solvent. Huang et al. reported a significant benefit of using ethanol as a solvent to serve as a capping agent to stabilize reactive phenol by alkylating with phenol-O and ring-C alkylation. This was reported to obtain 17 wt.% monomer with ethanol though under methanol the yield was only 6 wt.% [16], [17].

Rinaldi et al. demonstrated that one can obtain non-pyrolytic lignin bio-oil in 2-propanol/water with the presence of Raney Ni at 160°C. When the temperature increased from 160°C to 220°C, delignification increased from 53% to 87%. The authors claimed that the presence of water in the extracting medium improves the delignification. The water helps the transportation of the liquor into the biomass pellet. In comparison to the experiment, treating Organosolv lignin in the solvent mixture, the products from non-pyrolytic lignin bio-oil had shown a significant increase in bicyclic compounds [4].

Choi et al. studied different metals on carbon supports including Pt/C, Pd/C, Ru/C and Ni/C under supercritical alcohols. A combination of ethanol and Pt/C produced 77 wt.% of lignin-oil that mainly consists of 4-ethyl phenol, guaiacol, 4-ethyl guaiacol and syringol [18]. Commercial Pd/C and Ru/C catalysts yielded about 50% of phenolic monomers from birch wood in methanol. Sels et al. demonstrated that by changing from Ru/C to Pd/C, there is an increase in OH-content of the phenolic monomers products [19].

Table 2.1. Summary of recent reports on monomer yields over various solvents and catalyst.

Entry	Catalyst	Reaction Conditions			Yield of monomers	Reference
		Solvent	T (°C)	P (psi)		
1	Ru/C	H ₂ O	200	580	4	4.6 wt%
	Pt/C	H ₂ O	200	580	4	33.6 wt%
	Pt/C	dioxane/H ₂ O	200	580	4	41.7 wt%
2	MoC	Ethanol	280		6	47 wt%
3	Ru/C	Methanol	250	1750	3	48 C mol%
	Pd/C	Methanol	250	1750	3	49 C mol%
4	H-USY	H ₂ O/Methanol	250	100	0.5	47%

5	NiMO/Al ₂ O ₃	dimethyl	350	1450	4	14.8 wt%	[23]	
	CoMo/Al ₂ O ₃	disulfide	350	1450	4	10.8 wt%		
6	Pd/C	Methanol and H ₃ PO ₄	200	300	3	40.0 C mol%	[24]	
	Pd/C	Methanol and NaOH	200	300	3	25.0 C mol%		
∞	7	Ni/C	Methanol	200	500	3	24.5 wt%	[25]
	8	Ru/C	Methanol	200	500	4	16 wt%	[26]

2.2 Experimental

2.2.1 Catalyst Synthesis

5 wt.% Ru/SiO₂ was prepared using ruthenium chloride hydrate, RuCl₃·nH₂O (Sigma-Aldrich, 99.98%) by incipient wetness impregnation. After the impregnation, the catalyst was dried at 80°C overnight in the oven. The dry catalyst was calcined at 500°C in air at 100 ml/min for 4 hours.

2.2.2 Lignin Characterization

2D-NMR was performed on Varian VNMR 500 MHz instrument equipped with triplet resonance H-PFG probe. Solid sample was dissolved in DMSO-d₆ and measured using the inverse detected ¹H-¹³C correlation spectra (HSQC) at 25°C. HSQC experiment programmed with spectral widths of 5000 Hz (from 10 to 0 ppm) and 20,843 Hz (from 165 to 0 ppm) for ¹H and ¹³C dimensions, respectively. The number of complex points collected was 2048 for ¹H with a 1.5 second recycle delay. The number of transients was 64 and 256-time increments were recorded in ¹³C dimension.

2.2.3 Reaction Experiment and Product Characterizations

Lignin used in the depolymerization experiments was obtained from the filtration of stillage from bioethanol production provided by Abengoa Bioenergy. Experiments were carried out in 50-mL Parr reactor. Lignin depolymerization was performed using 500 mg of starting material and 20 mL of solvent at 280°C and 1400 psi of H₂. In the case of biomass experiment, 1 gram of Red Oak with 20 mL of ethanol was carried out at 280°C under approximately 1400 psi of hydrogen. Prior to running reaction, the system was charged with N₂ three times to remove air, then 400 psi of H₂ was charged at room

temperature. The reaction time started once the temperature controller reached 280°C. The mixture was stirred at 600 rpm. The reaction was stopped with rapid cooling to room temperature before the gas was discharged. The mixture was filtered. The residue was dried overnight and weighed. The difference between the initial mass and the final residue weight was taken as lignin disappearance.

The filtrate was filtered again through a 0.2 μm syringe filter before analyzing in gas chromatography. GC-MS and GC-FID are equipped with DB-1701 column (60 m x 0.25 mm x 0.25 μm). 2 mL of filtrate was dropped on 200 mg of silica and stirred. The solid was dried in the oven at 80°C to remove the ethanol solvent. The solid was pyrolyzed in Pyroprobe unit to study the liquid products that could not be detected in GC-MS/FID.

Raw oak, the residue after oak depolymerization and the liquid after oak depolymerization trapped in SiO_2 were pyrolyzed using CDS Analytical Pyroprobe 5250T apparatus with autosampler. Between 0.5 mg to 1.0 mg of sample was loaded into a quartz tube with a filler rod and quartz wool packed below to prevent the sample from falling out the bottom (Figure 2.1). The quartz tube with filler rod and quartz wool was weighed before and after the sample loading. After the samples were loaded on the autosampler and GC signal ready, the carousel dropped the sample tube into the pyrolysis chamber. Then, the chamber was purged with helium for 20 seconds to remove any air. Following this purge, the filament was heated to the set point. The evolved vapors passed through a valve oven heated to 300°C then swept into the transfer line that was connected to the injection port of the attached gas chromatography. Once the gas chromatography was completed, the filament was deactivated and the valve was opened to allow the

sample to drop by gravity out of the chamber. The pyrolysis chamber was cleaned by reactivating the filament to 1200°C and held for 20 seconds while purging with helium. The vapors from pyroprobe pyrolysis were analyzed in an online Shimadzu QP2010 GC-MS/FID system fitted with a RTX-1701 column (60 m x 0.25 mm x 0.25 μm).

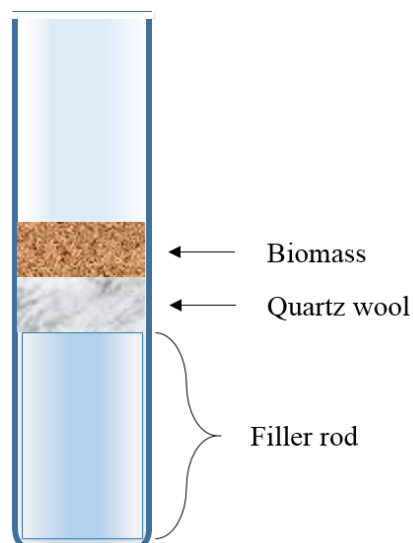


Figure 2.2. Quartz tube for pyroprobe pyrolysis.

Identification of the product peaks in all the experiments was based on the library search as well as literature resources previously published by Felix et al. [27]. Quantification of the products in all cases was calculated using effective carbon number (ECN) model corresponds to each target molecule and its relative response factor in the gas chromatography. ECN model was introduced by Sternberg et al. to which it takes into account the number of carbons in the molecule that are effective in producing FID signal.

ECN value depends on the structure and the functional groups of the molecule. The model was developed and validated with 42 compounds based on the typical

functionalities in pyrolysis bio-oil, including sugar derivatives, light oxygenates and phenolic. The ECN contributions of each functional category are shown in Table B1.

The structural characterization was examined using X-ray diffraction (XRD) and scanning electron microscope (SEM). SEM characterizing was done on ZEISS NEON High Resolution with Schottky emitter electron source. For XRD characterization, a D8 Series II X-ray diffractometer (Bruker AXS) was determined in reflection geometry using CuK α radiation generated at 40 kV and 35 mA in the 2 θ range from 2° to 70°.

2.3 Results and Discussion

2.3.1 Lignin Depolymerization

In order to depolymerize the lignin successfully, it is necessary to break the linkages. This will generate oligomers that can undergo several reactions and transform into monomeric products. However, oligomers and unsaturated monomers can undergo repolymerization. Alcohols have been demonstrated to be excellent solvents for biomass depolymerization due to their hydrogen transferability.

Table 2.2. Lignin Disappearance in methanol and ethanol solvent at different temperatures.

	Methanol		Ethanol	
Temperature (°C)	280	80	220	280
Lignin Disappearance (%)	57	58	75	95

Table 2.2 shows a comparison of lignin disappearance between methanol and ethanol solvent. Lignin disappearance was calculated by the difference between the initial weight of lignin dry basis and the unreacted lignin after filtration on the dry basis. After 12 hours

of treating the lignin at 280°C in hydrogen, 57% of solid lignin disappeared, while in ethanol, it can solubilize the lignin up to 95%. Surprisingly, ethanol was able to solubilize 58% of the lignin when it was stirred at 80°C overnight but no monomer was detected. Once the reaction temperature was increased to 220°C, almost 75% of stillage lignin disappeared but the only 1-2% of monomers were detected. When the supercritical temperature of ethanol (280°C) was applied, up to 7% of monomers were detected. This demonstrated that both methanol and ethanol are good solvents and they are capable to extract the lignin even at low temperature. However, at a lower temperature, most of the solubilized lignin were large dimers or oligomers that could not be detected by GC-MS/FID. Overall, ethanol is better to solubilize lignin than methanol.

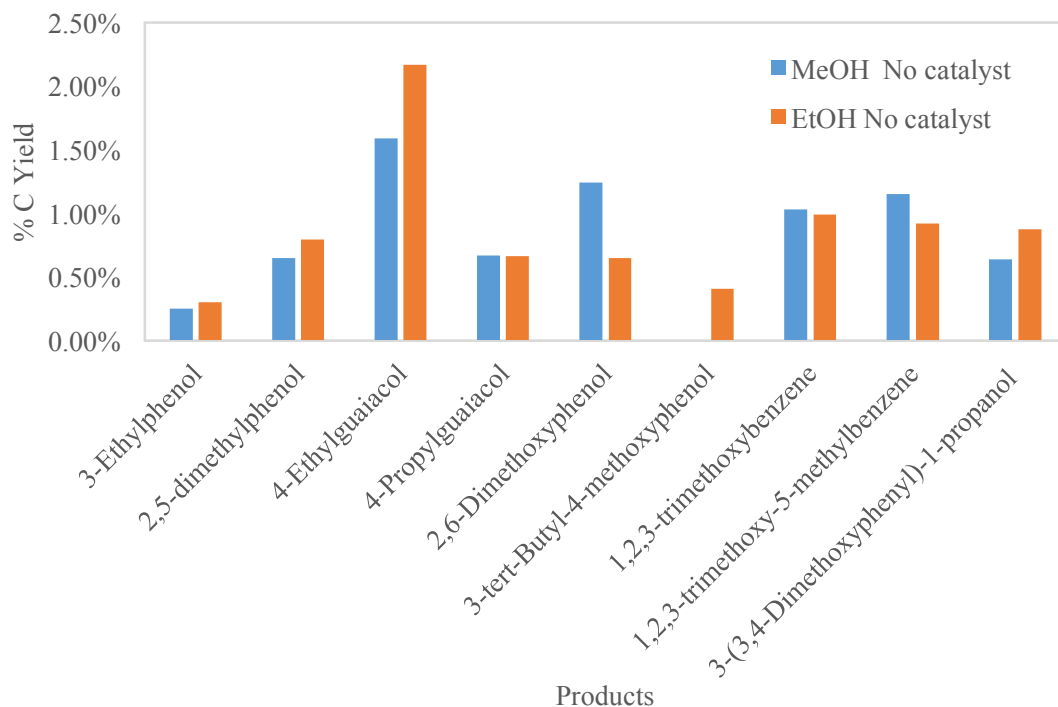


Figure 2.3. Percentage of monomers yield from methanol and ethanol at 280°C, 1500 psi H₂ and 12 hours.

From Figure 2.3, the monomers that were detected from both methanol and ethanol solvents were similar and the yields of the monomers were about the same. The total yields of the monomers were approximately 7% from nine monomers that were able to identify. These monomers are 3-ethylphenol, 2,5-dimethyl phenol, 4-ethylguaiacol, 4-propylguaiacol, 2,6-dimethoxyphenol, 3-tert-butyl-4-methoxyphenol, 1,2,3-trimethoxybenzene, 1,2,3-trimethoxy-5-methylbenzene and 3-(3,4-dimethoxyphenyl)-1-propanol. In both cases, the major product was 4-ethylguaiacol. As mentioned earlier that the disappearance of the lignin was as high as 90% in the supercritical ethanol but only a total of 7% C yield of monomers, this reinforces that the lignin was depolymerized into dimers and oligomers. When GC-MS and GC-FID results of the same experiments were compared, it is obvious that more than 9 peaks between 30-60 minutes of retention

times were detected. However, due to its complexity and the concentration of the products, other peaks could not be identified and were marked as unknown. Although that ECN model could estimate the unknown, it may lead to underestimating/overestimating of the yield.

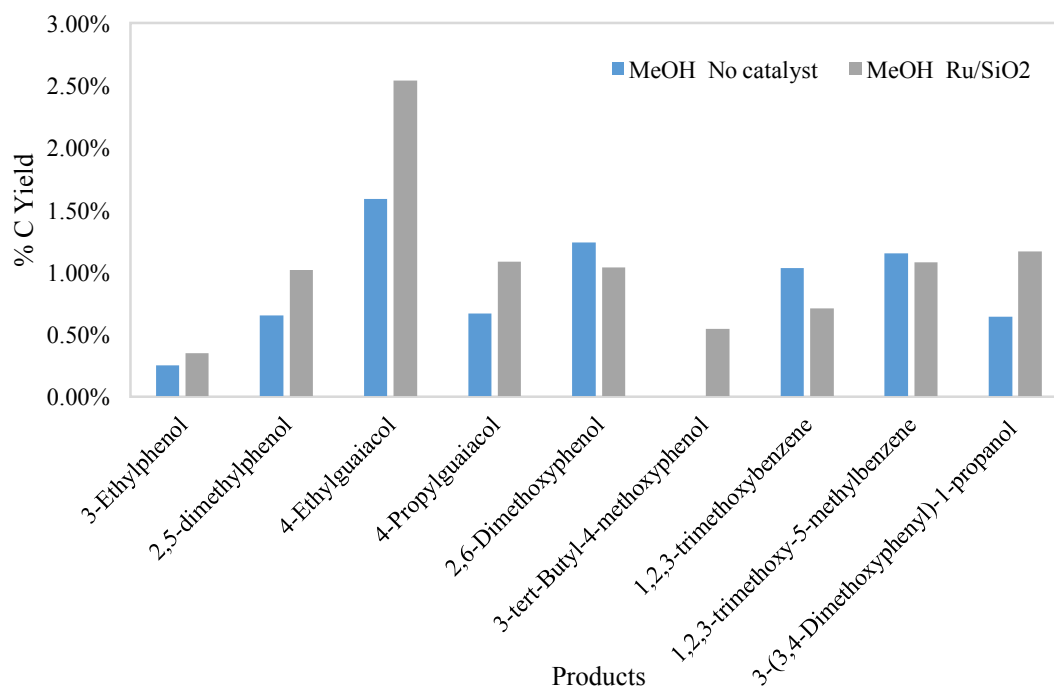


Figure 2.4. Percentage of monomers yield from methanol with or without Ru/SiO₂ at 280°C, 1500 psi H₂ and 12 hours.

Ethanol was the choice of the solvent in this research project as it can be obtained from bio-ethanol plants and due to its low boiling point, it could easily be removed from the liquid mixtures prior to the second catalytic upgrading step. As a good hydrogen donor, ethanol helps to solubilized and break hemicellulose and lignin in the biomass.

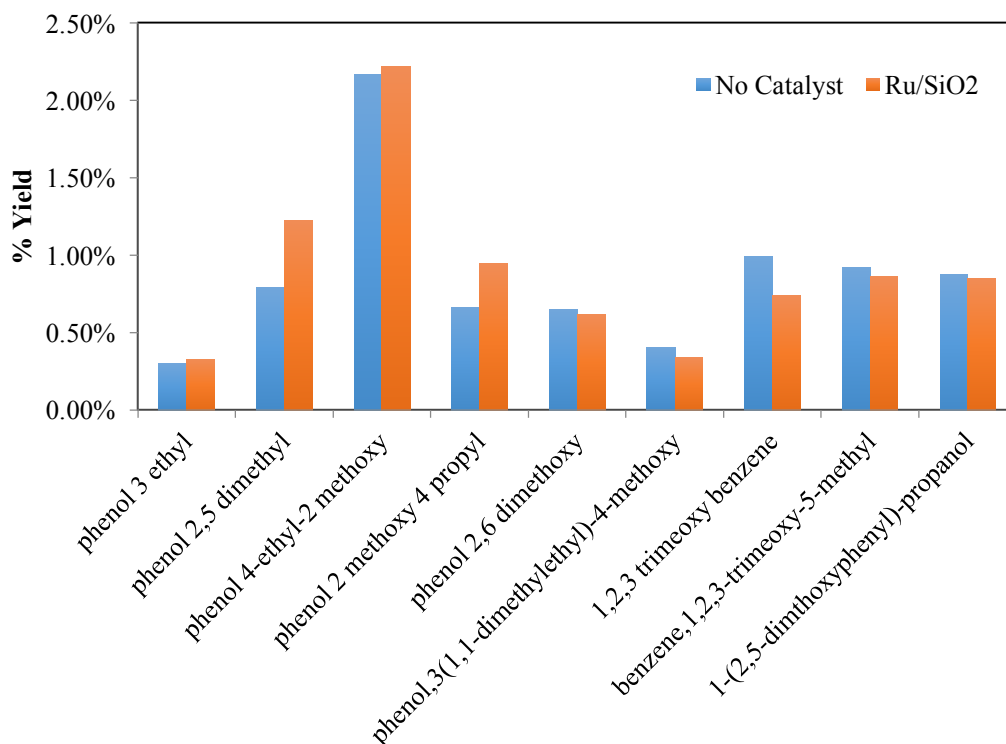


Figure 2.5. Percentage of monomers yield from ethanol with or without Ru/SiO₂ at 280°C, 1500 psi H₂ and 12 hours.

Figure 2.5 shows the monomers yield from ethanolysis of lignin with and without the catalyst at 280°C and 1400 psi H₂. The yield of monomers was no difference. In both scenarios, the disappearance of lignin was more than 90%. When feeding non-pyrolytic lignin soup with fresh Ru/SiO₂ catalyst and ran the reaction at 280°C and 1400 psi H₂, there was no increase in the yield of monomers. B. Gomez-Monedero et al. observed similar results to ours regarding the monomers yield from lignin reaction with and without catalysts [26].

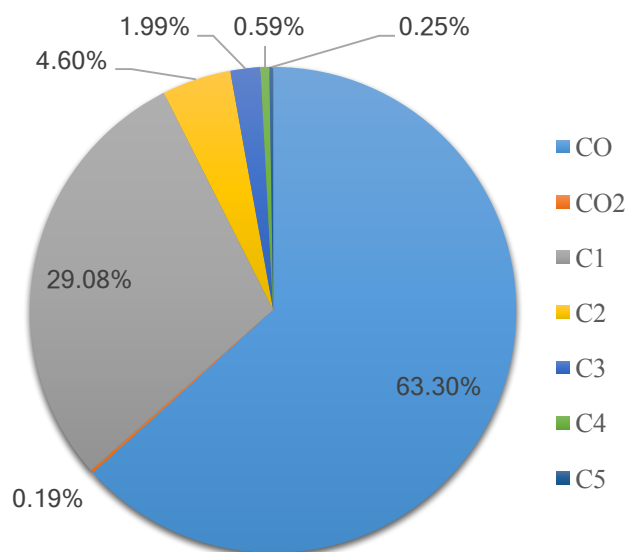
In literature, the terms “lignin oil”, “bio-oil” or “product oil” are all ambiguous without defining the definition or clarification of how the yield was calculated. Not only that literature ignored the fact that without the tools to quantify the lignin oil, it may lead

to overestimating of the yield, but only a few literatures from the best of my knowledge that had reported a blank or a controlled reaction of the lignin. Therefore, this has been misleading that when the solid catalysts were fed with the biomass, the catalysts helped to convert the solid biomass to monomers bio-oil.

2.3.2 Ethanol Conversion over Ru/SiO₂

To understand the role of the solvent and the catalyst, a series of studies on ethanol and Ru/SiO₂ alone was conducted. One observation with the ethanol under supercritical conditions is that not only does ethanol helps to break the bond of the lignin polymer by hydrogen transfer but ethanol also reacts forming other by-products. Products of ethanol conversion are shown in Figure 2.6. The major liquid product is acetaldehyde via the dehydrogenation of ethanol. Aldol condensation of acetaldehyde followed by dehydration and hydrogenation yielded butanal. Diethyl ether is emerging from two molecules of ethanol. Two C6 by-products from ethanol conversion are diethoxy ethane and diethyl acetate. Diethoxy ethane was formed through acetalization of acetaldehyde and ethanol. Ester formation is derived from the carboxylic acid reacts with the alcohol. However, acetic acid was not detected in the product. This means that under the reaction condition, the oxidation of ethanol to acetic acid immediately reacts with ethanol to ethyl acetate.

(a)



(b)

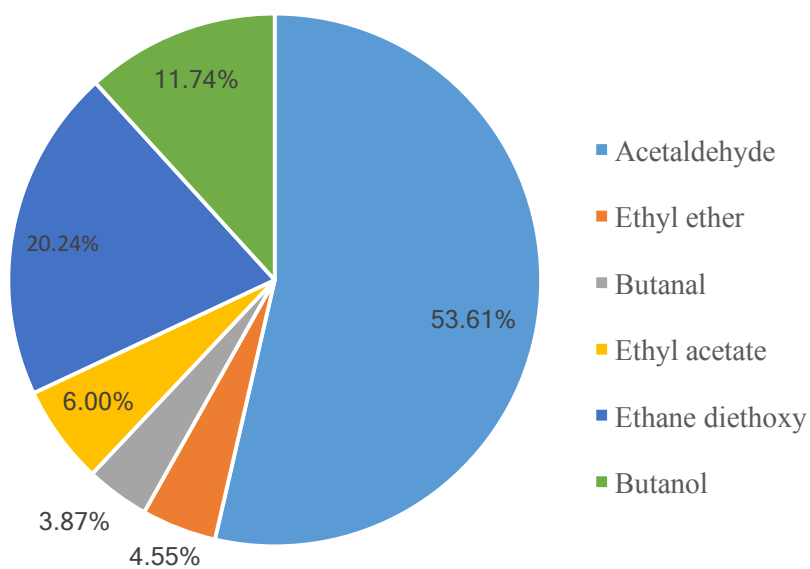


Figure 2.6. Selectivity from the conversion of ethanol over Ru/SiO₂ (a) gas products selectivity and (b) liquid products selectivity.

Not only ethanol produced liquid products but also light gases were detected. The major gas product was carbon monoxide and methane. The little amount of C2 to C5 gases was observed. A trace of carbon dioxide was detected as well. This implies that ethanol is likely gone through dehydrogenation to acetaldehyde then decarbonylation to form methane and carbon monoxide. At this point, we can conclude that Ru/SiO₂ is active in the ethanol reaction.

Ru/SiO₂ catalyst from the reaction of lignin in ethanol was filtered and dried then recycled with fresh ethanol. The spent catalyst had lost most of its activity but it was still able to dehydrogenate forming acetaldehyde. However, the acidity that needed for other products were lost. This could be from the coking of lignin that killed the activity of the catalyst.

The abundance of the ethanol is another reason that there was no enhancement in the monomeric products with the addition of the catalyst. Ethanol would competitively adsorb on the ruthenium sites that prevent the adsorption of the oligomers. Ethanol forming acetaldehyde also condensates to large molecules that could also block the active sites.

Table 2.3. Mole of products from the conversion of ethanol over (a) Ru/SiO₂, (b) Ru/SiO₂ and lignin, (c) spent catalyst from reaction (b) and (d) without catalyst only lignin.

Liquid Phase Products	Mole of Products			
	(a) Ethanol + Ru/SiO ₂	(b) Ethanol + Ru/SiO ₂ (250 mg) + Lignin	(c) Ethanol + Spent Catalyst from (b)	(d) Ethanol + Lignin (no catalyst)
Acetaldehyde	5.57E-03	7.82E-03	3.53E-03	1.25E-03
Ethyl ether	2.36E-04	3.22E-04	-	1.45E-04
Butanal	2.01E-04	2.18E-04	-	-
Ethyl acetate	3.11E-04	1.79E-04	-	-
Diethoxy ethane	7.00E-04	1.10E-03	3.09E-04	2.77E-04
Butanol	6.10E-04	1.09E-03	-	-
Total	7.62E-03	1.07E-02	3.84E-03	1.68E-03

2.3.3 Carbon content in the catalyst after the reaction

After the reaction, unreacted lignin and the solid support/catalysts were separated by filtration. The residue was dried in the oven at 80°C overnight to remove ethanol. The carbon content of the residue was analyzed by elemental analysis. In the reaction, the known amount of solid support or catalyst was subtracted from the total initial solid weight (lignin + SiO₂ or Ru/SiO₂) to determine the amount of unreacted lignin. The carbon content in the liquid was taken as the remaining from the carbon content in unreacted lignin and/or the catalyst.

The raw lignin was found to have 61% of carbon composition. After the reaction with only ethanol, the amount of carbon in the unreacted lignin was 44%, which means 56% of carbon content from the original lignin was solubilized in ethanol. With an addition of SiO₂ in the system, lignin disappearance increased to 78.8% and the amount of carbon that was trapped in the silica was 17%. This would give a 62% carbon content in the liquid lignin oil.

Table 2.4. Carbon content of lignin residues after ethanolysis.

Conditions	% Lignin Disappearance	% Monomer Yield	%C		
			Unreacted Lignin	Catalyst	Filtrate liquid
Ethanol without Catalyst	56.8	7.78	44	-	56
Ethanol with SiO ₂	78.8	7.16	21.0	17.0	62
Ethanol with Ru/SiO ₂	97.0	8.15	2.0	5.9	92

In the reaction with Ru/SiO₂, lignin disappearance increased to 97% and the carbon content found in the catalyst was 6%. In every reaction with or without the catalyst, the monomer yields were similar (7-8 %) even though that catalyst could be helping with the cleaving of the linkages in the lignin. But they only resulted in large trimers or oligomers that were trapped inside the catalysts, thus deactivated the active species for later depolymerization to monomers.

2.3.4 NMR study on lignin

The solids obtained after the experiment were analyzed in 2D NMR. The chemical shifts at 3.3 to 4.2 ppm (¹H) and 55 to 57 ppm (¹³C) was assigned to methoxy group (-OCH₃). Guaiacyl unit was identified in the region 6.5 to 7.0 ppm (¹H) and 115 to 117 ppm (¹³C) and in the lower region 5.9 to 6.5 ppm (¹H) and 118 to 122 ppm (¹³C). The peak region 6.4 to 6.8 ppm (¹H) and 104 to 107 ppm (¹³C) was assigned to syringyl unit. P-hydroxyphenyl was centered in the region of 6.6 to 7.1 ppm (¹H) and 125 to 130 ppm (¹³C). Also, p-coumarate was observed in the region 7.1 to 7.3 ppm (¹H) and 125 to 130 ppm (¹³C). The ether bonds, β-o-4 and β-o-β' were assigned in the region of 4.8 to 5.4 ppm (¹H) and 65 to 75 ppm (¹³C) and 4.5 to 4.7 ppm (¹H) and 65 to 70 ppm (¹³C) [26].

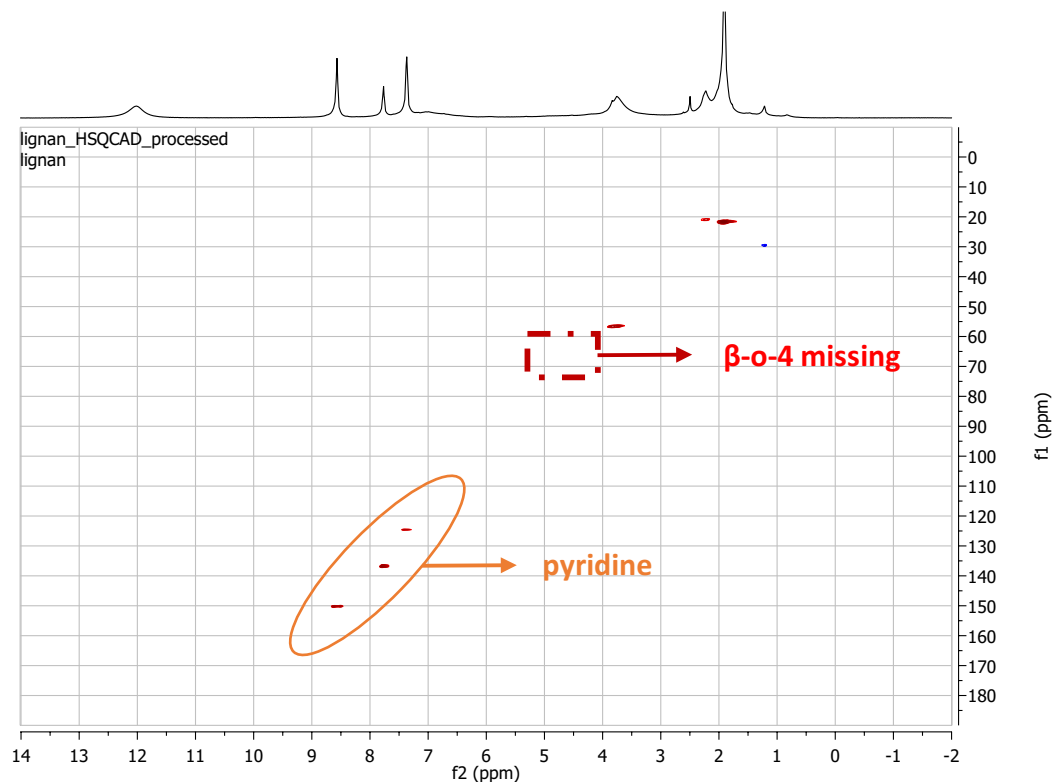
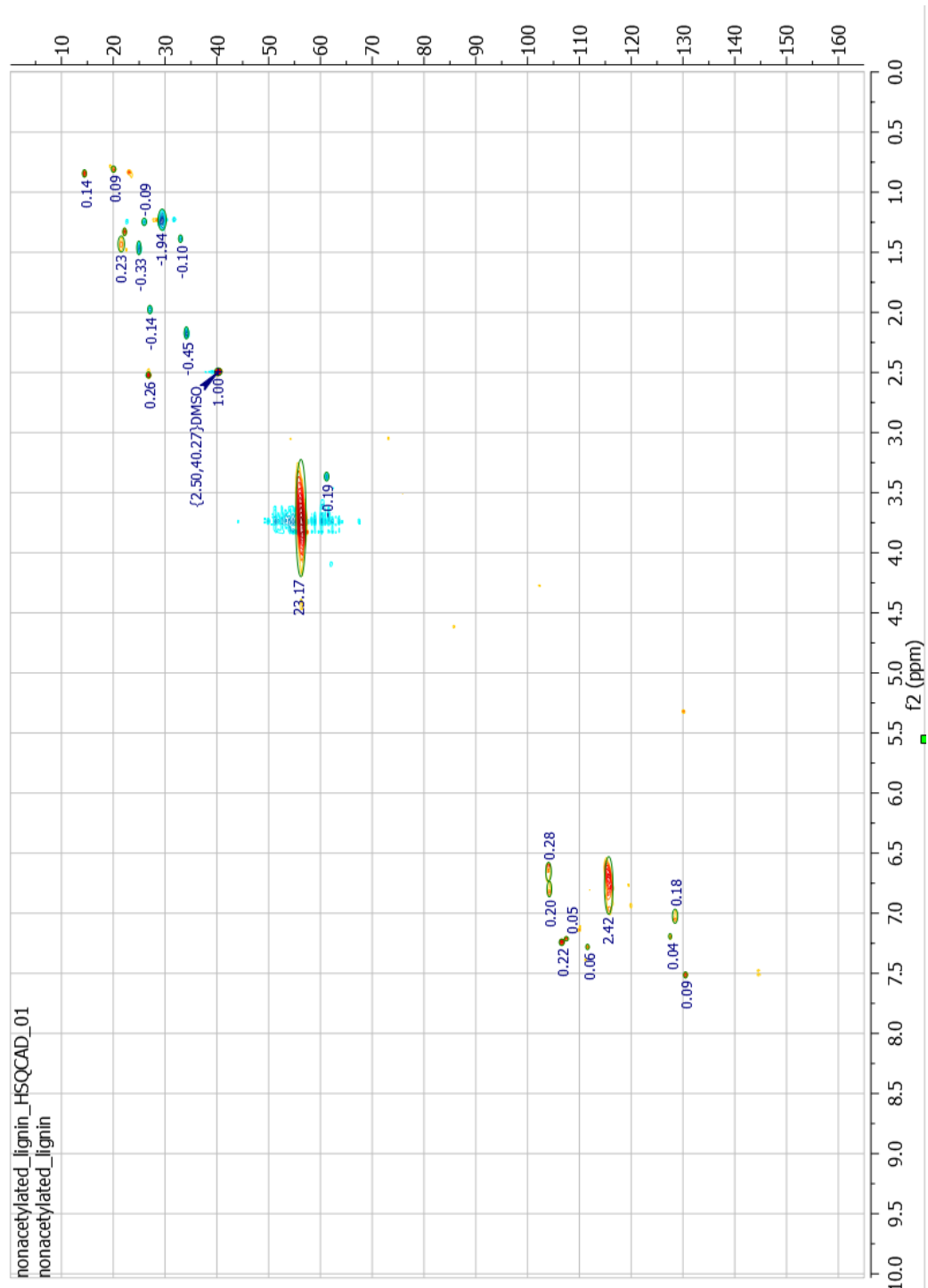


Figure 2.7. 2D-HSQC of acetylated lignin sample.

Normally, lignin samples are acetylated before 2D-NMR using acetic anhydride and pyridine as a solvent. The acetylation is required to avoid fractionation of the material and increase the solubility and the chemical shift dispersion of the side chain units. After the acetylation, the sample requires to remove excess pyridine and acetic anhydride by the freeze-drying method. However, due to the limitation of the instrument, we were only able to dry the sample using rotary evaporator followed by liquid nitrogen trap. As seen in 1D of ^1H -NMR on Figure 2.7, protons on the pyridine are assigned at 7.23, 7.61 and 8.59 ppm which are seen in the acetylated samples. This shows that our drying method was not efficient to remove all the pyridine and remained at high concentration. This

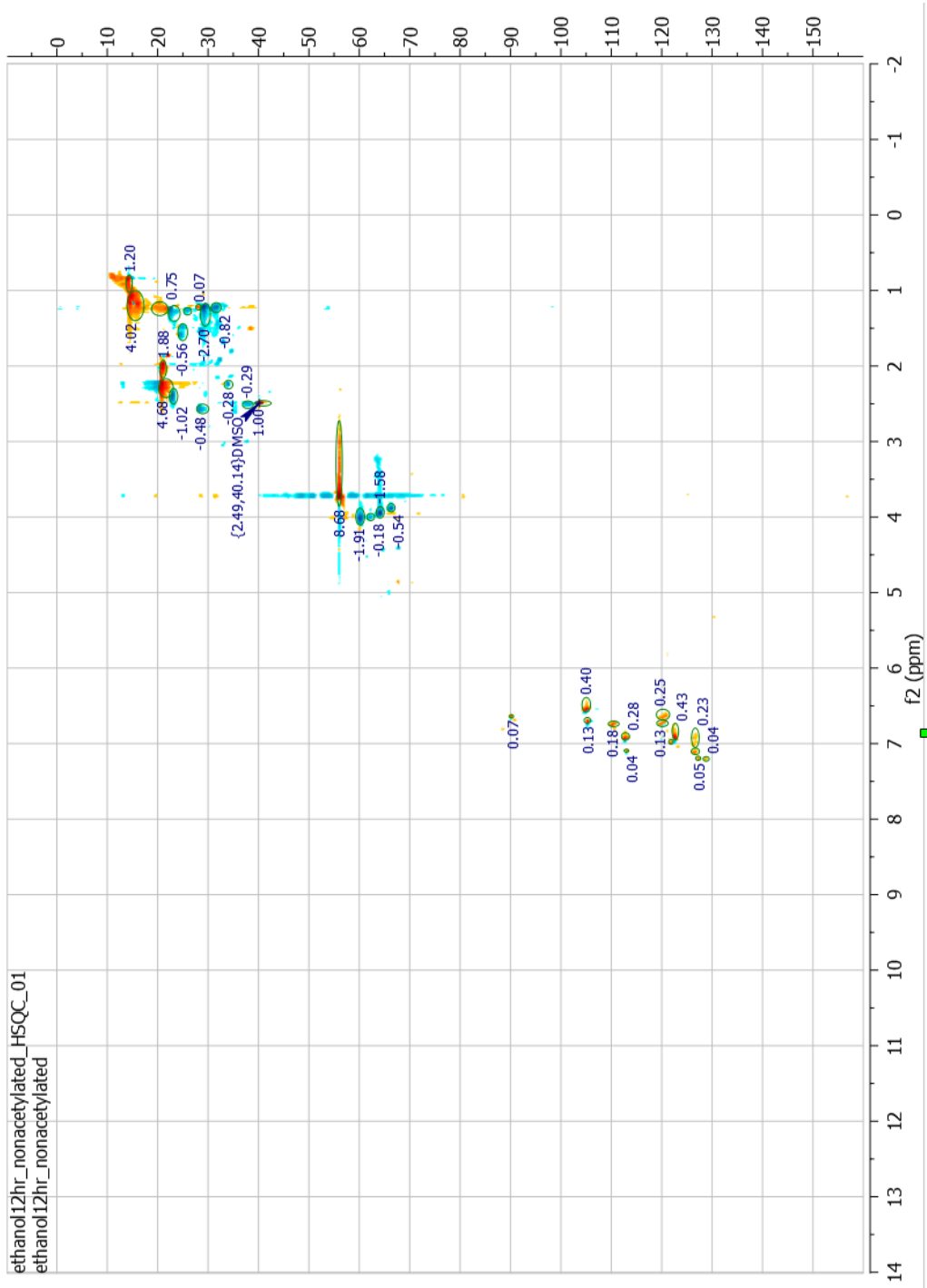
results when analyzed in 2D-NMR mode causing the characteristics of all the functional groups and linkages described above to be blinded by the pyridine peaks. From this onwards, the samples of the lignin were only studied in NMR without acetylation.

From 2D-NMR results, all the ether C-O linkages, β -o-4 and β -o- β' , and other linkages in the lignin were not observed. Therefore, the extent of linkage disappearance could not be calculated. One remarkable observation from the integration of 2D-NMR before and after the reaction is the methoxy group (-OCH₃), assigned at 3.3 to 4.2 ppm (¹H) and 55 to 57 ppm (¹³C). The methoxy group was greatly reduced after the reaction. Methoxy group/DMSO-d₆ ratio had gone from 23.17 in the untreated lignin to 9.15 in the residual after the reaction with Ru/C. The ratio of S/G and S/H also showed to slightly increase after the reaction.



(a)

(b)



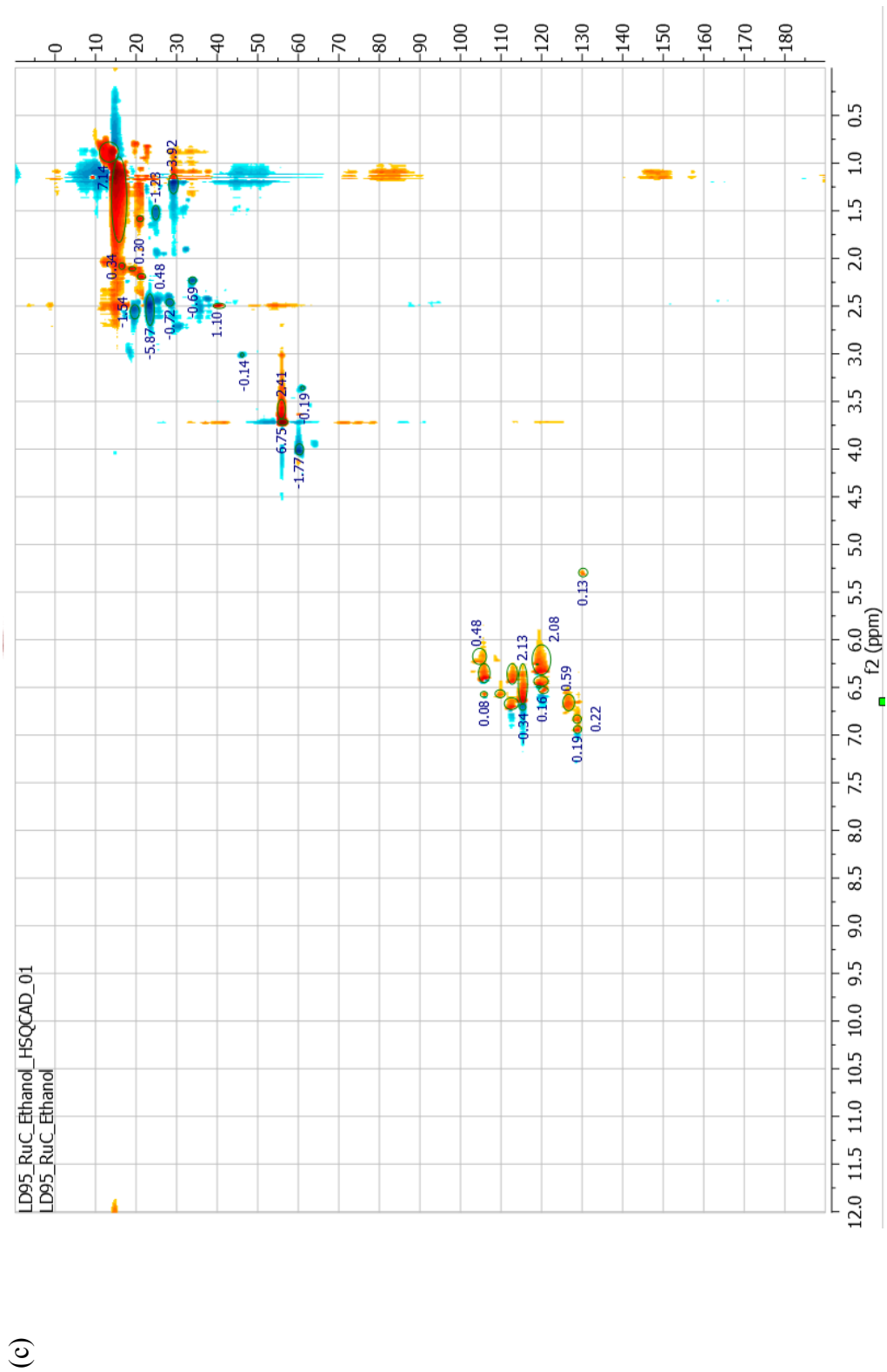


Figure 2.8. 2D-HSQC NMR spectrum from (a) untreated lignin, (b) ethanol treated and (c) ethanol treatment over Ru/C

2.3.5 Red Oak Ethanolysis

From a better understanding of the alcoholysis in lignin leads to a question of alcoholysis in biomass. As mentioned earlier that biomass composes of cellulose, hemicellulose, and lignin and conventional technology that uses to convert biomass to valuable chemicals is pyrolysis. This technique decomposes the biomass at elevated temperature to produce bio-oil that requires further treatment to capture any large oligomers. The aim of biomass ethanolysis is to simplify the process and use the ethanol as the media to attack the cell wall of the biomass. Not only that the ethanol has shown to be an excellent source of solvent in the previous research but ethanol itself produces from biomass fermentation process. Figure 2.15 proposes the strategy of using ethanol to produce non-pyrolytic bio-oil to the upgrading steps. Biomass is fermented to produce ethanol that is used in the ethanolysis process to dissolve and stabilized the bio-oil. Because of the macromolecules products that could blind the active sites or form coke in the catalyst in the latter catalytic process, bio-oil should be treated with silica trap. The silica trap is then pyrolyzed at a higher temperature to break heavy molecular weight compounds to high-value chemicals. The liquid left after trapping should be extracted to an organic phase so that ethanol can be recycled back and also avoided the conversion of ethanol in upgrading step.

From XRD results in Figure 2.9, raw oak composes of three distinct peaks at 2θ of 15° , 22° and 35° . The diffraction peak at 15° could be assigned to the amorphous parts of the cellulose while the peak intensity at 2θ of 22° represent (002) lattice plane of cellulose which represented both crystalline and amorphous parts of the cellulose. The peaks

observed at $2\theta = 35^\circ$ could be assigned to (040) lattice planes of cellulose [28], [29]. The cellulose crystallinity was calculated based on the following formula:

$$CI(\%) = \frac{(I_{22^\circ} - I_{15^\circ})}{I_{22^\circ}} \times 100\%$$

The XRD diffraction of the oak sample from ethanol treatment at 80°C shows similar diffraction peaks to the raw oak suggesting that the surface morphology of red oak was unchanged and the crystalline cellulose structure was preserved. Cellulose crystallinity was 42% in the raw oak and 40% from the treatment at 80°C . This phenomenon is supported by SEM image seen in Figure 2.10 with the biomass surface remained rough and uneven. However, when the treatment temperature increased to 280°C under a high pressure of hydrogen, the surface of the biomass became smoother with small granular particles precipitated on the surface. These particles seen on SEM images could be the precipitation of dimers and oligomers during cooling down of the reaction. The XRD diffraction at 280°C demonstrates the structure of the residue became amorphous. This indicates that cellulose crystallinity was destroyed during the ethanol treatment.

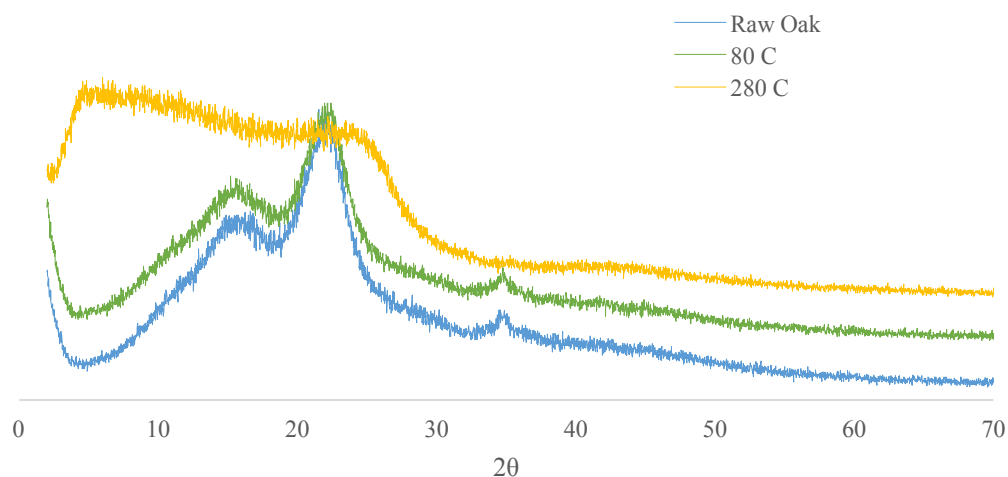


Figure 2.9. XRD of (a) raw oak, (b) ethanol treatment at 80°C and (c) ethanol treatment at 280°C.

From these results, we can explain the phenomena of how the biomass depolymerizes in ethanol. Cellulose has a crystalline structure whereas hemicellulose is less defined and has an amorphous structure. On the other hand, lignin is a network of aromatic polymer. Figure 2.11 illustrates that as the temperature rises, ethanol that acts as a hydrogen donor penetrates into biomass, lignin starts to break down. At 280°C, dimers, and oligomers are formed and more cellulose and hemicellulose are broken. During the cooling down, the temperature decreases, some of dimers and oligomers precipitate and deposit on the surface of biomass, which appears like small granules on the SEM image.

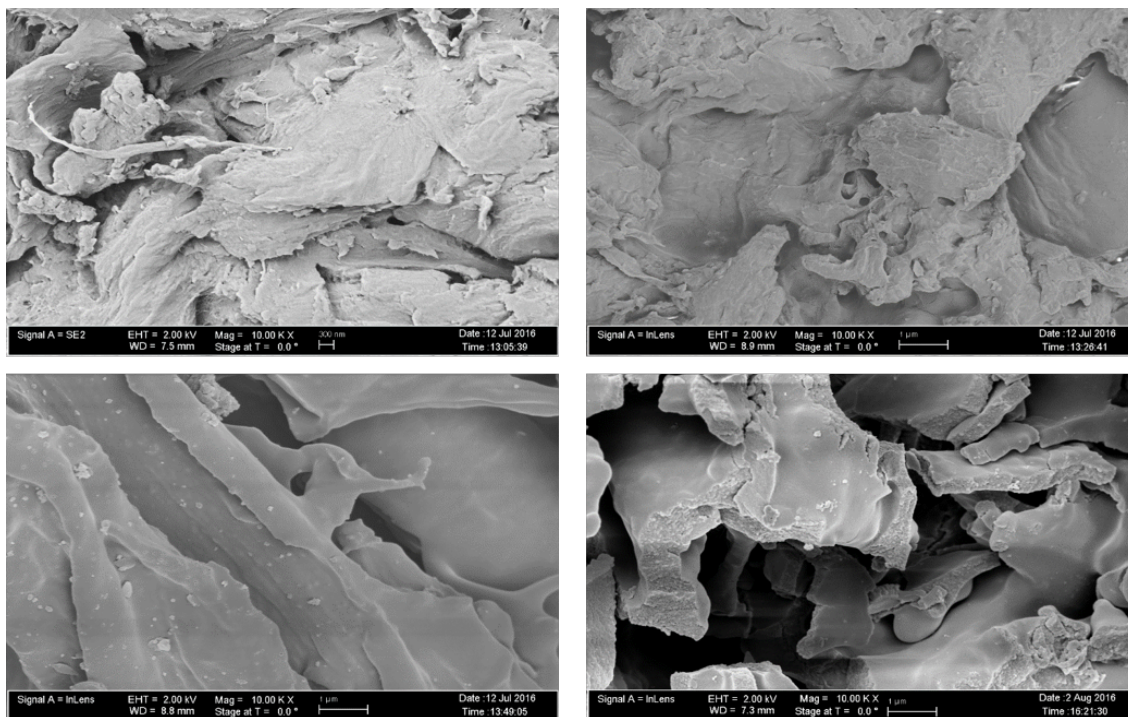


Figure 2.10. SEM of raw oak (top left), ethanol treatment at 80°C (top right) and ethanol treatment at 280°C (bottom left and right).

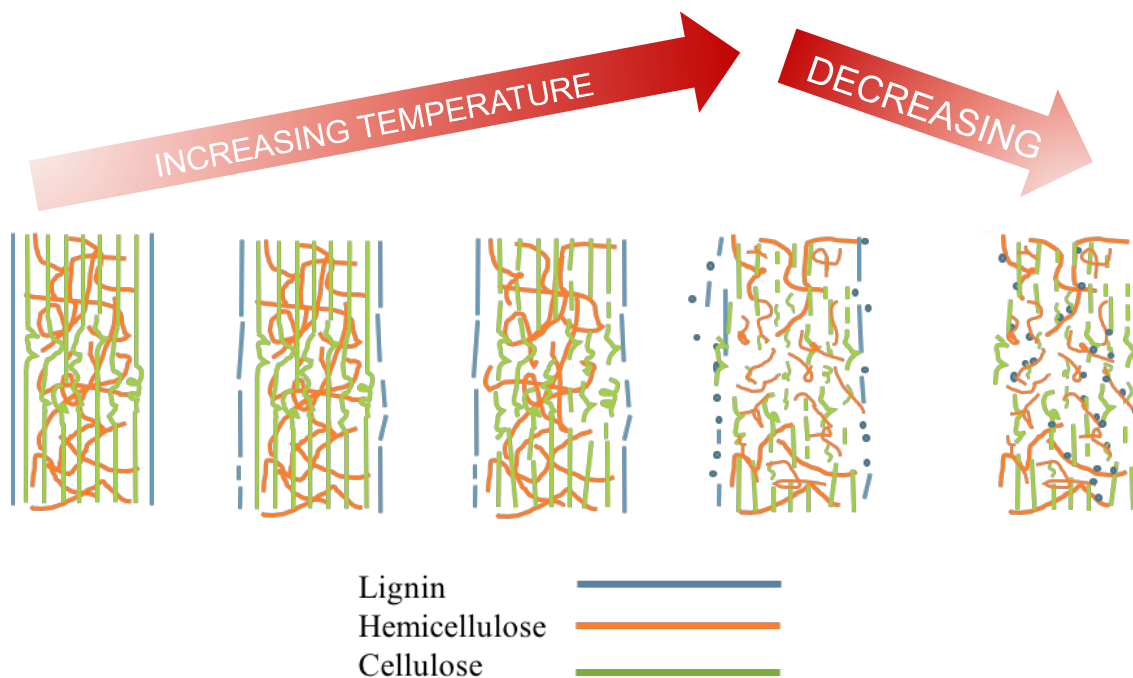


Figure 2.11. Schematic of the breaking down of cellulose, hemicellulose, and lignin in red oak treating ethanol.

2.3.6 Pyrolysis study of oak residue

After ethanolysis reaction, the liquid was filtered. Any unreacted biomass or residue was dried in the oven at 80°C for 12 hours to remove excess ethanol. The residues from red oak ethanolysis were pyrolyzed in the pyroprobe unit connecting to online GC-MS/FID at 520°C for 60 seconds.

The results of the oaks residues from the ethanolysis reaction at 250°C and 280°C are shown in Figure 2.12 The peaks were categorized into different compound groups, namely, acetic acid, acetone, furans, furans derivatives, light oxygenates, methoxy phenols, sugars, light gases and others. The results show that both temperatures have similar product selectivity despite the fact that after the reactions the disappearance at

250°C was only 57%, but up to 80% of red oak were lost at 280°C. The solid residue after ethanolysis mostly contained sugar derivatives having a selectivity of 60%. This suggests that the difference from the ethanolysis temperature only breaks down more oak, but does not change any the compositions of the residue.

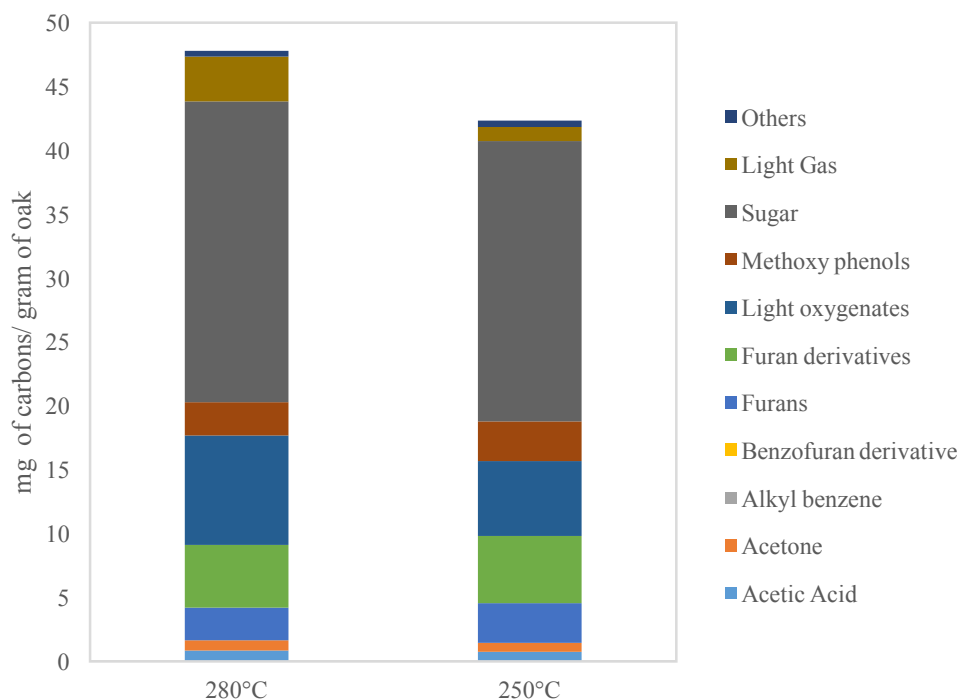


Figure 2.12. Carbon yields from pyroprobe of residue from oak treatment in ethanol at 250°C and 280°C. Conditions: 520°C for 60 seconds.

According to Figure 2.13, the yields from the residues of oak ethanolysis is similar to the stage 3 thermal fraction. Thermal fractionation was developed to produce several products streams from low temperature to high temperature. C. Waters et al. studied the fractionation at three different temperatures; 270°C, 350°C and 520°C. At low temperature (270°C) or so-called stage 1 torrefaction, the major liquid products are water

and light oxygenated compounds. The residue of stage 1 torrefaction is collected and pyrolyzed at 350°C. The products obtained at this temperature is called stage 2 torrefaction. In stage 2, levoglucosan constitutes 16.2% of the total liquid product. Some water and acetic acid were also seen at this stage, suggesting remaining unreacted hemicellulose. Stage 3 was carried out at 520°C using the stage 2 solid residue. As seen in Figure 2.13, the majority of the products stream compose of anhydrous sugar and methoxy phenols. Levoglucosan, which derived from cellulose observed in stage 3, suggests that cellulose decomposition was incomplete. Phenolic species is much expected at stage 3 from the decomposition of lignin [30].

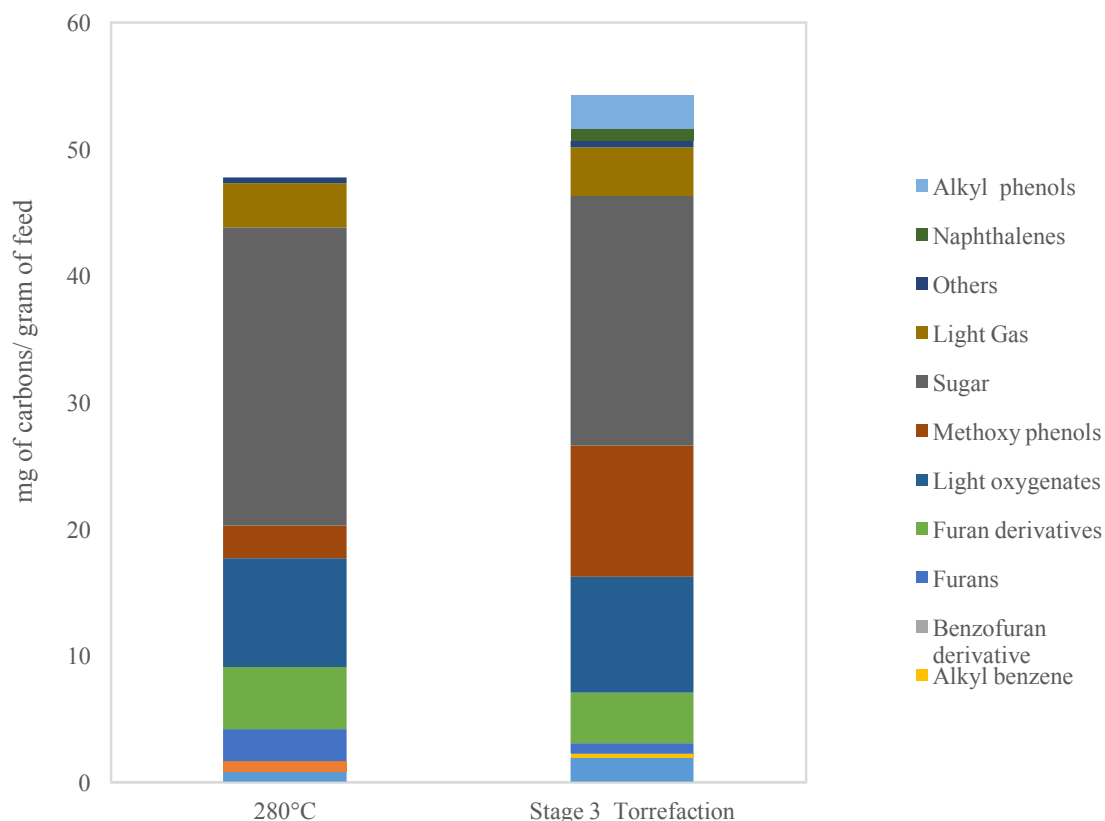


Figure 2.13. Carbon yields from pyroprobe of residue from oak treatment in ethanol at 280°C and Stage 3 torrefaction (520°C for 60 seconds).

The similarity between the residue of the oak ethanolysis and the stage 3 torrefaction implies that during ethanolysis, some of the hemicellulose and lignin should have been attacked, leaving mostly cellulose in the biomass. As mentioned before that the liquid products from oak ethanolysis, only traces of monomers were observed. Therefore, almost all dissolved molecules were heavy oligomers that cannot be detected by FID. The liquid products were trapped in silica support and pyrolyzed in pyroprobe at 520°C. The results show that almost 60% of the selectivity were light oxygenates compound namely acetaldehyde. About 13% of methoxy phenols and only 1% of furan derivatives were seen in the product stream. According to this result, much of the lignin was attacked and solubilized in ethanol in the form of oligomers.

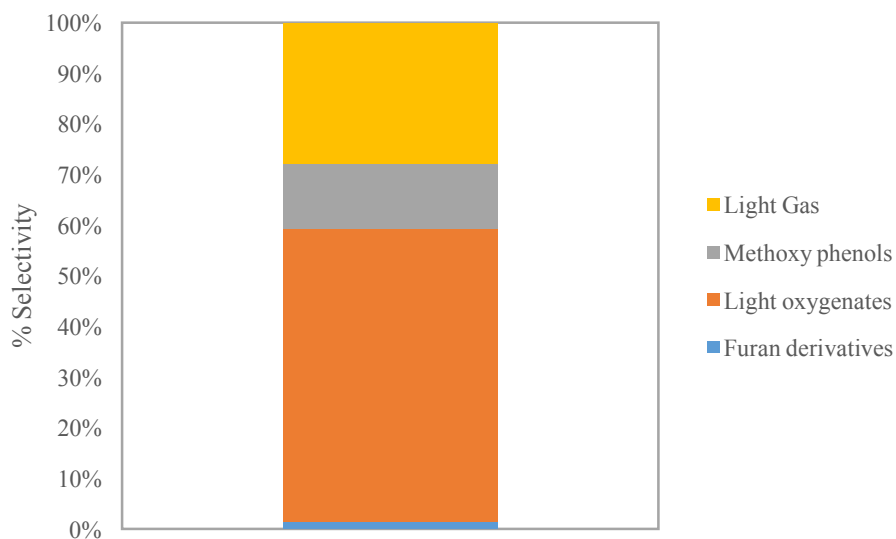


Figure 2.14. Liquid products from oak ethanolysis pyrolyzed at 520°C.

From these results of biomass ethanolysis and lignin ethanolysis in the previous section, we have seen ethanol can effectively solubilize polymers complex by breaking down the chains into the smaller structure. However, the non-pyrolytic bio-oil composed

of large oligomers that require separation and treatment before upgrading to high-value chemicals.

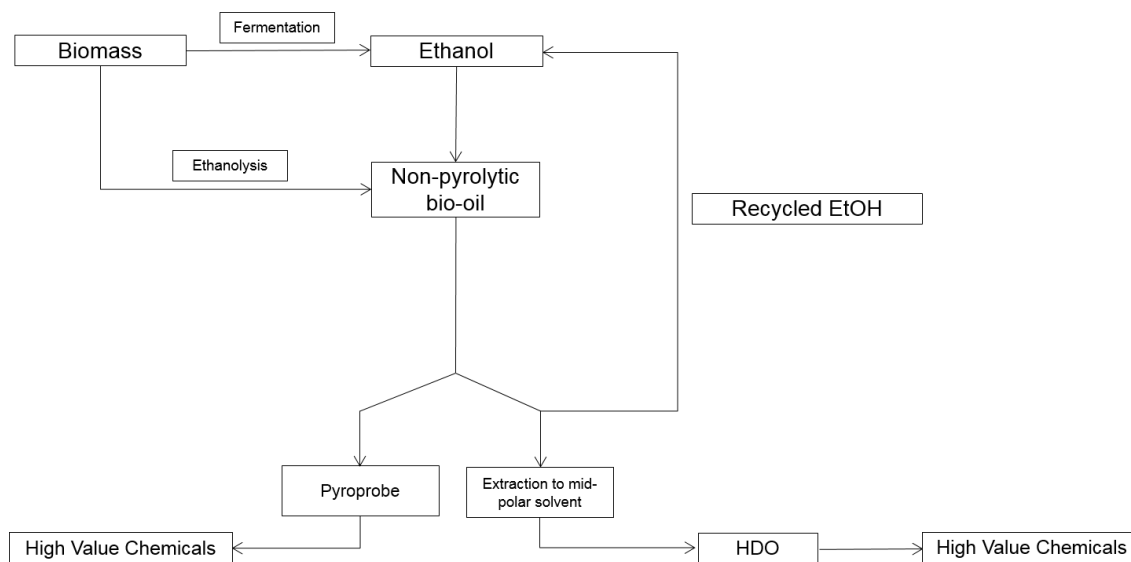


Figure 2.15. Proposed process strategy of the ethanolysis from extracting biomass to non-pyrolytic bio-oil to the high-value chemicals upgrading.

2.4 Conclusions

From the study of lignin ethanolysis, the results have shown that methanol and ethanol can successfully solubilize the lignin. Ethanol can be used more effectively in terms of industrial application as it is produced from the fermentation of biomass. However, we have observed that the addition of the catalyst did not increase the yield of monomers which suggests that large fraction of the liquid are oligomers and require severe treatment to trap these oligomers before further upgrading. The same goes for the oak ethanolysis that only traces of monomers were detected in FID.

XRD and SEM results of oak ethanolysis show that at 280°C treating, the morphology of the oak have completely changed and mostly oak have lost much of its crystallinity. According to pyroprobe studies of the residue, the products show similar selectivity to

stage 3 torrefaction suggesting that the lignin partially decomposes in ethanol and most cellulose and hemicellulose were retained.

Chapter 3. Hydrogenation of Diphenyl Ether over Ru/SiO₂

This chapter is a (to be published) Puridej Warakunwit and Daniel Resasco's paper.

3.1 Introduction

With an increasing demand for energy and the environmental issues arise, biofuels energy deriving from biomass has gained much attention. Lignocellulosic biomass contains cellulose, hemicellulose, and lignin. Depending on the source of the biomass, the contents of each constitutes vary. There are different ways and strategies to upgrade the biomass to valuable biofuels and chemicals. Pyrolysis of biomass yields a viscous mixture of bio-oil that contains hundreds of compounds. Bio-oil usually contains up to 20-40 wt.% of oxygen. Conventional strategies to increase the energy density of pyrolytic bio-oil is first deoxygenating to reduce the reactivity of the feedstock then selectively upgrade the platform molecules to other fuels and chemicals. Pyrolysis of biomass results in recalcitrant lignin meaning that aromatics polymer are more connected through carbon-carbon bonds [1]–[3].

The most abundant linkages in lignin are β -O-4, β -5, 5-5, β - β , β -1 and 4-O-5. The bond dissociation energy (BDE) of C-C bond in the lignin linkage is as high as 384 kJ mol⁻¹ while BDE of C-O bond is much weaker (220-314 kJ mol⁻¹). Among C-O linkage in the lignin, 4-O-5 is the strongest ether bond with BDE of 314 kJ mol⁻¹ [31]–[33]. Breaking this C-O bond linkage is a challenge. Nevertheless, the 4-O-5 units are formed by the coupling of oligomers during the depolymerization. Therefore, lignin after acidic treatment would contain more of 4-O-5 linkages [6].

Solid catalysts such as Ni-based and Pd-based have shown to cleave the aromatic ethers bond of lignin in the aqueous medium. Other heterogeneous organometallic catalysts such as Ni(COD)₂ have been reported to cleave C-O bonds in diaryl ether [34], [35]. J. He et al. calculated the initial TOFs and the apparent activation energies of different 4-O-5 compounds over 57 wt.% Ni/SiO₂. The initial TOF of 4,4'-dihydroxydiphenyl ether was almost three times higher than that of diphenyl ether. This could be due to the two hydrophilic hydroxyl groups in 4,4'-dihydroxydiphenyl ether can enhance the solubility in water and the adsorption capability on the metal site. Different substituents on diaryl ethers lead to different reaction pathways for cleaving C-O bonds. Diphenyl ether cleaves C-O bonds via the combination of hydrogenolysis and hydrolysis, surface hydrogenolysis conversion for diphenyl ether and hydrogenolysis for di-p-tolyl ether [36].

Rinaldi et al. studied the solvent effect on the hydrogenolysis of diphenyl ether over Raney Ni under 50 bar H₂ at 363 K. The conclusion drawn from this study are that conducting the reaction in the solvents with Lewis basicity such as methanol and THF is less active but highly selective towards aromatic products, phenol and benzene. On the other hand, nonpolar solvents such as decalin and n-heptane show a high conversion and high selectivity to cyclohexyl ether, cyclohexanol, and cyclohexane. This implies that the solvent plays an important role to hydrolyze the lignin. Using polar and Lewis basic solvent can dissolve lignin but they can decrease the activity of the catalyst. Instead, using non-polar solvents that maximize the activity of Raney Ni cause difficulty to the solubility of lignin [37][38].

In order to depolymerize the lignin, the linkages must be broken. The most abundant linkage in the lignin is the ether bond, therefore, the depolymerization of the lignin should correlate with the oxophilicity of the metal catalysts. According to the DFT calculations performed by Qiaohua T. et al., the metal-O bond strength (oxophilicity) increases in the order Pt<Pd<Rh<Ru<Fe. The oxophilicity of the metal is a direct function of the d-band center and how close the d-band band center to the Fermi level will determine the M-O bond strength. This is because as the d-band center is closer to the Fermi level, the antibonding orbital of the hybridization between the metal and oxygen is further away and thus results in a less electron occupancy. Then, the M-O bond becomes stronger and the metal is more oxophilic [39], [40][41]. With these reasons, the metal Ru was chosen because it has an intermediate oxophilicity that can catalyze the C-O bond cleavage in the lignin linkages.

3.2 Experimental

3.2.1 Catalyst Synthesis and Characterization

5 wt.% Ru/SiO₂ was prepared using ruthenium chloride hydrate, RuCl₃·nH₂O (Sigma-Aldrich, 99.98%) or ruthenium (III) nitrosyl nitrate in dilute nitric acid solution, Ru(NO)(NO₃)₃ (Sigma Aldrich, 1.5%) by incipient wetness impregnation. After the impregnation, the catalyst was dried in the oven at 80°C overnight. The dry catalyst was calcined at 673 K in air at 100 ml/min for 4 hours. Pt/SiO₂ was prepared with the same procedures as Ru/SiO₂ catalyst using tetraamineplatinum nitrate, [Pt(NH₃)₄](NO₃)₂ (Alfa Aesar, 99.995%) precursor.

The reduction temperature of the catalyst was carried out in temperature-programmed reduction (TPR). 50 mg of catalyst sample was heated in 5% H₂/Ar (35 sccm) from the ambient temperature at a rate of 10 K min⁻¹ to 973 K while the amount of H₂ consumption was monitored with a thermal conductivity detector (TCD). Fourier-transform infrared spectroscopy (FTIR) was carried out in a Perkin-Elmer Spectrum 100 equipped with a high-temperature DRIFT (diffuse reflectance infrared Fourier transformation) cell with CaF₂ windows. The sample was pretreated in-situ at 523 K for 2 hours under H₂ flow (30 mL/min) to reduce the catalyst. The cell was cooled down to 323 K before pyridine was bubbling with He flow for 30 mins. The sample was flushed under the flow of He to remove weakly adsorbed pyridine for 1 hour. Then the DRIFT spectra were collected 64 times with a resolution of 1 cm⁻¹.

3.2.2 Reaction Experiment

All experiments were carried out in 50-mL Parr Reactor. In a typical experiment, 25 mg of catalyst and 20 mL of decalin (Sigma Aldrich, 99%) were loaded into the reactor. The reactor was purged with N₂ three times, then pressurized with H₂ to 200 psi to reduce the catalyst. After the reduction, the system was cooled down to 343 K to inject diphenyl ether (Sigma Aldrich, ≥99%) diluted in decalin from a pressurized feeding cylinder then pressurized the reactor to 700 psi of H₂. The zero reaction time started once the temperature reached the set temperature. After the reaction, the reaction was stopped by a rapid cool down with ice bath. The catalyst was removed via filtration. The analysis was done using a Hewlett Packard 6890 GC-FID equipped with DB-1701 column (60 m x 0.25 mm x 0.25 μm) for quantification, while a Shimadzu QP2010 GC-MS equipped with ZB-1701 column (60 m x 0.25 mm x 0.25 μm) was used for products identification.

In all the runs the carbon balance was better than 95%. Diphenyl ether conversion and selectivity in carbon basis are defined as followed:

$$\% \text{ conversion} = \frac{\text{initial mole of diphenyl ether} - \text{final mole of diphenyl ether}}{\text{initial mole of diphenyl ether}} \times 100\%$$

$$\% \text{ selectivity} = \frac{\text{carbon mole of products}}{\text{carbon moles of diphenyl ether converted}} \times 100\%$$

3.3 Results and Discussion

3.3.1 Catalyst Characterization

The reduction temperature of ruthenium was measured by temperature programmed reduction (TPR). Figure 1 shows a single sharp peak of 5% Ru/SiO₂ appeared at 470 K. This peak suggests the reduction of Ru oxide particles to metallic Ru.

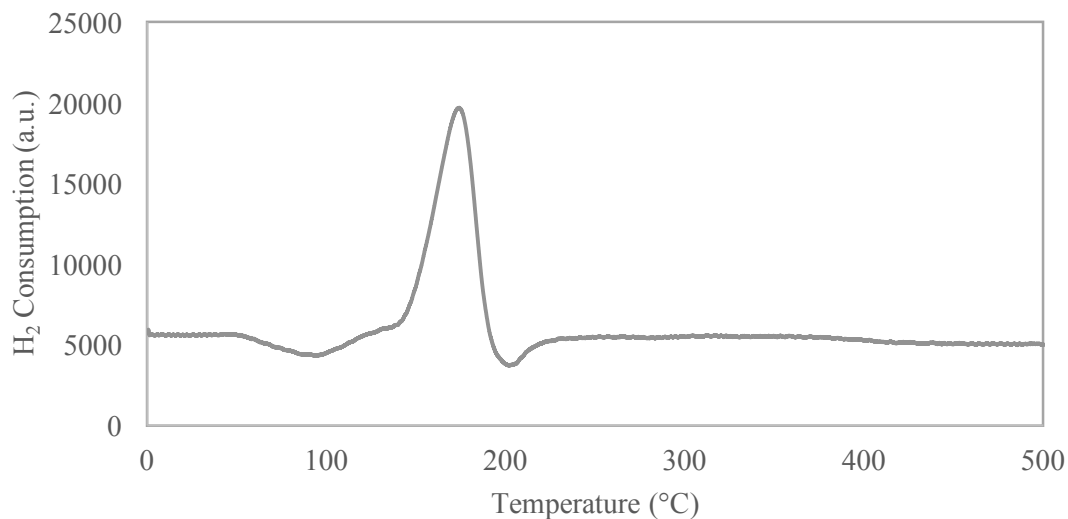


Figure 3.1. TPR of Ru/SiO₂.

FTIR spectra of adsorbed pyridine on Ru/SiO₂ prepared by ruthenium(III) chloride precursor is shown in Figure 3.2. Two adsorption bands at 1440 and 1583 cm⁻¹ were

observed. These bands were assigned to Lewis acid sites, which is in good agreement with the literature [42]–[44]

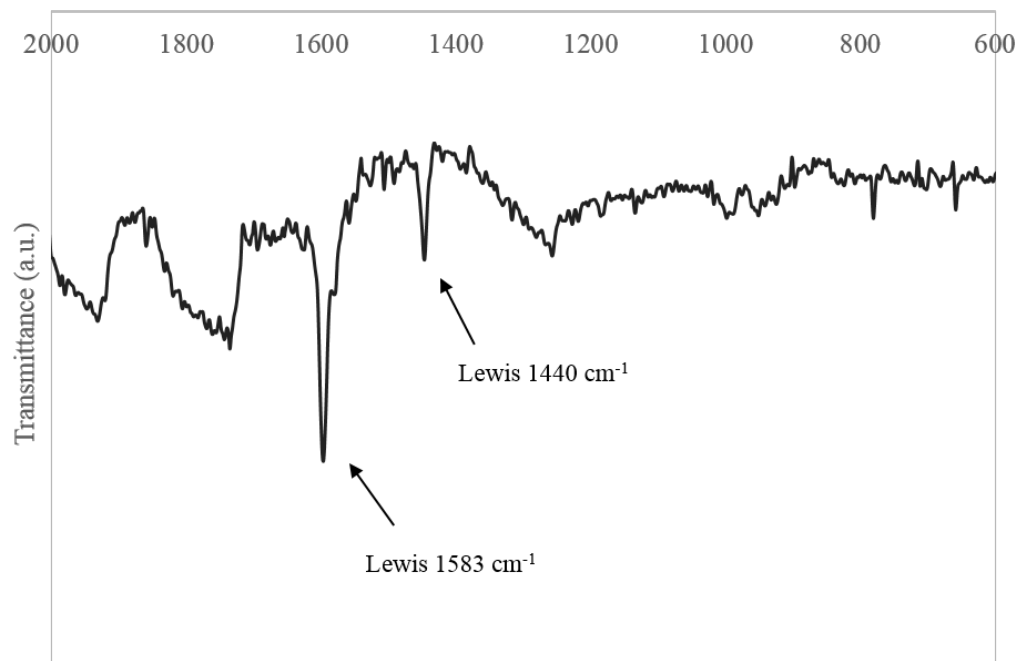


Figure 3.2. FTIR of Ru/SiO₂

3.3.2 Catalytic Performance of Ru/SiO₂

Catalytic performance of diphenyl ether was performed in decalin. This organic solvent was chosen due to two main reasons. First, diphenyl ether has low solubility in the aqueous phase and secondly decalin is stable under the reaction conditions. The temperature of the reaction on Ru/SiO₂ was performed at 363 K.

Table 3.1. Conversion of diphenyl ether at different reaction temperatures.
Reaction conditions: 0.15 M diphenyl ether, decalin (25 mL), 5 MPa H₂, 500 rpm.

Catalyst	Conversion (%)		
	333 K	363 K	423 K
1% Pt/SiO ₂	NA	0	22
1% Rh/SiO ₂	94	100	NA
5% Ru/SiO ₂	NA	76	NA

Catalytic performance on diphenyl ether hydrogenation was examined on three different metals on a silica support. Both 1% Rh/SiO₂ and 5% Ru/SiO₂ show good activity. After one hour of reaction, the conversion reaches 94% in 1% Rh/SiO₂ at 333 K. 5% Ru/SiO₂ converts 76% of diphenyl ether at 363 K. 1% Pt/SiO₂ observes no activity at 363 K and sees 22% of conversion at 423 K. However, when we fed toluene to Pt/SiO₂ at 333 K, toluene converted 23% to methylcyclohexane. This suggests that diphenyl ether may have adsorbed stronger on Pt site thus no activity was observed at a lower temperature.

Both 1% Rh/SiO₂ and 1% Pt/SiO₂ observe similar and expected hydrogenation products: cyclohexyl phenyl ether, cyclohexyl ether, cyclohexane, and cyclohexanol. 5% Ru/SiO₂ reactions also yield these hydrogenation products and unexpectedly 2-cyclohexyl cyclohexanone, which is a bicyclic C-C molecule, was observed. Typically, the formation of C-C molecules needs acid sites to catalyze while in a metal on silica support do not possess acidic character. From this observation, it implies that the 5% Ru/SiO₂ may have a unique characteristic that allows carbon-carbon molecule formation. The characteristic and the pathway of bicyclic molecule formation on 5% Ru/SiO₂ will be discussed below.

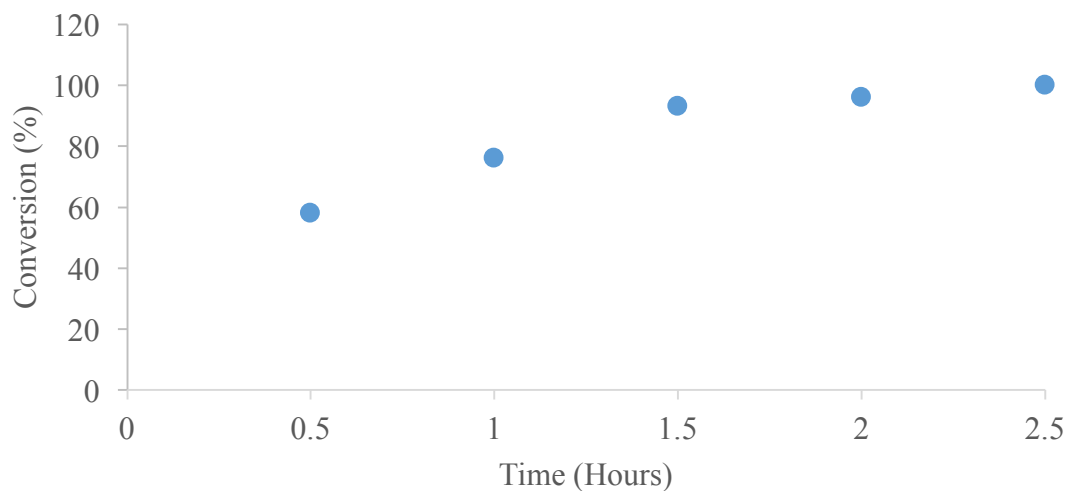


Figure 3.3. Conversion of diphenyl ether over 5% Ru/SiO₂ at a different time.

As seen in Figure 3.3 after 30 minutes, 58% diphenyl ether converted and the reaction reached 100 % conversion within 2.5 hours. The major product at 30 minutes is cyclohexyl phenyl ether (Figure 3.4). After 2 hours of reaction, all cyclohexyl phenyl ether hydrogenated to cyclohexyl ether. Hence, at higher conversion, cyclohexyl ether is dominated. Hydrogenolysis of cyclohexyl ether to cyclohexane and cyclohexanol is slow and remains almost the same. Unexpectedly, 6-9 % yield of 2-cyclohexyl cyclohexanone and a trace amount of 2-cyclohexylidenecyclohexanone were observed.

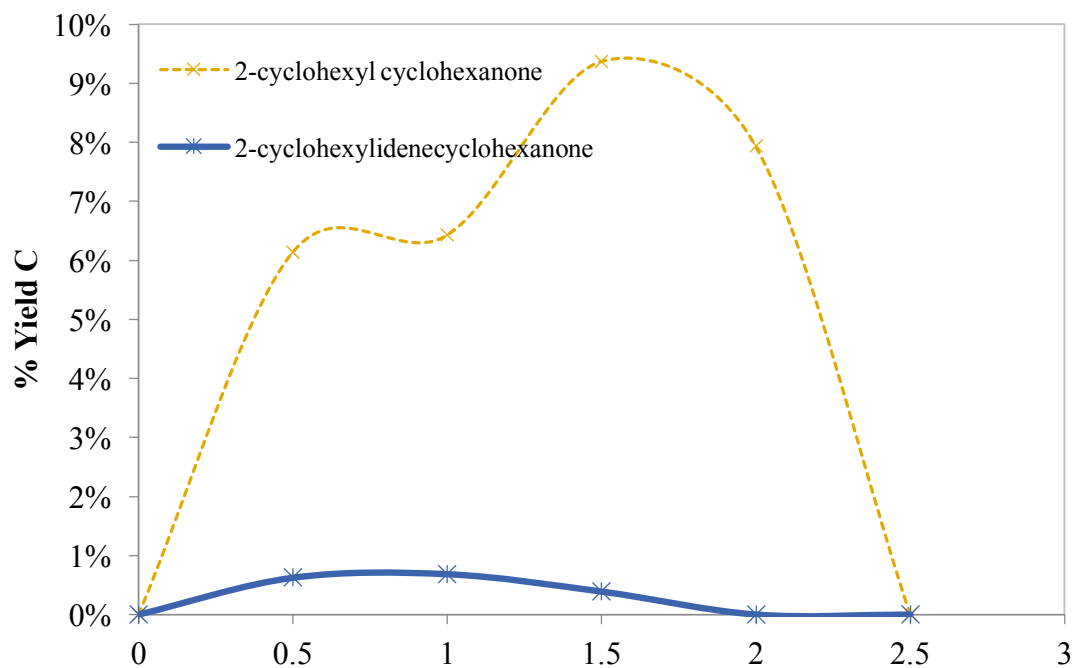
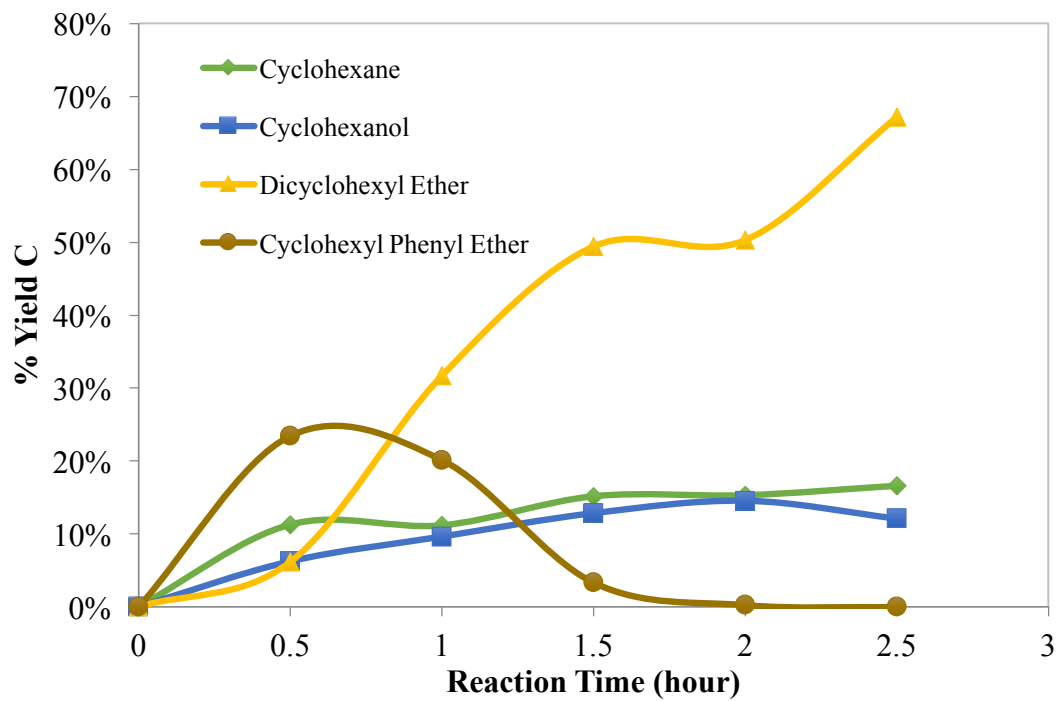


Figure 3.4. Product yield over different time.

In order to understand the primary and secondary products of the reaction, the reactions followed product distribution at different amount of catalyst and fixed the

reaction time at 30 mins. Figure 3.5 shows conversion and products distributions with increasing the catalysts from 12.5 mg to 50 mg. The conversion increased from 65% to 85%. By increasing the amount of catalysts, the primary product, cyclohexyl phenyl ether gradually decreases while the secondary product, cyclohexyl ether, triples. Even though there is a significant increase in the saturated bicyclic ring but the yields of cyclohexane and cyclohexanol only observe slight increase. This implies that ether C-O bond breaking is limited by the saturation of the ring. 2-cyclohexyl cyclohexanone was observed with a maximum value of 8% yield at 50 mg Ru/SiO₂ and only a trace amount of 2-cyclohexylidencyclohexanone was seen.

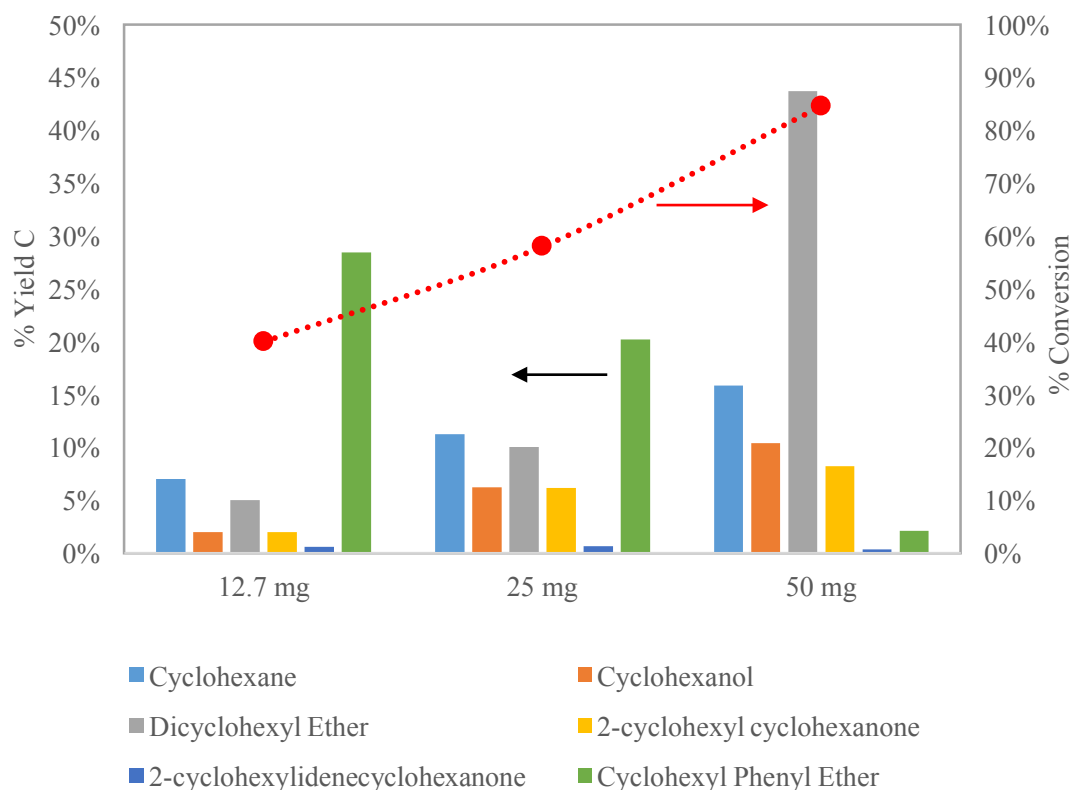


Figure 3.5. Conversion of diphenyl ether and products yield over a different amount of catalyst.

He et al. observed that C-O bond was cleaved from diphenyl ether in Ni/SiO₂ forming benzene and phenol but phenol immediately hydrogenated and was not observed in their final products [36]. In our study, benzene and phenol were not observed even at a short reaction time. From Figure 3.5, the result suggests that C-O ether cleave at C_{benzene}-O_{ether} forming phenol and cyclohexane. Phenol rapidly hydrogenated resulting cyclohexanol.

From this results, the proposed reaction pathway is shown in Figure 3.7. Diphenyl ether first hydrogenates to cyclohexyl phenyl ether. If the second ring hydrogenated, cyclohexyl ether forms. When the C-O bond breaks, monomer molecules, cyclohexane, and cyclohexanol are produced. Under the acidic environment, diphenyl ether forms C-C dimer molecules, cyclohexyl cyclohexanone. This C-C dimer molecules forms via carbon-carbon rearrangement or via alkylation.

3.3.3 Bicyclic molecules formation

The carbon-carbon bond formation can be catalyzed by the acidity. There are two possibilities to the acid catalyzed reaction. The first one is the acidity is coming from the support. The second reason is coming from the ruthenium. To assure that the bicyclic molecules occurred on ruthenium acid sites, an experiment on 5% Ru/TiO₂ prepared by ruthenium (III) chloride was performed. With the same experimental conditions as the silica support, 5% Ru/TiO₂ had shown similar products distributions and also showed the C-C molecules. This indicates that these products happened on Ru metal site and that the supports (silica nor titania) should have no effect on the reactions.

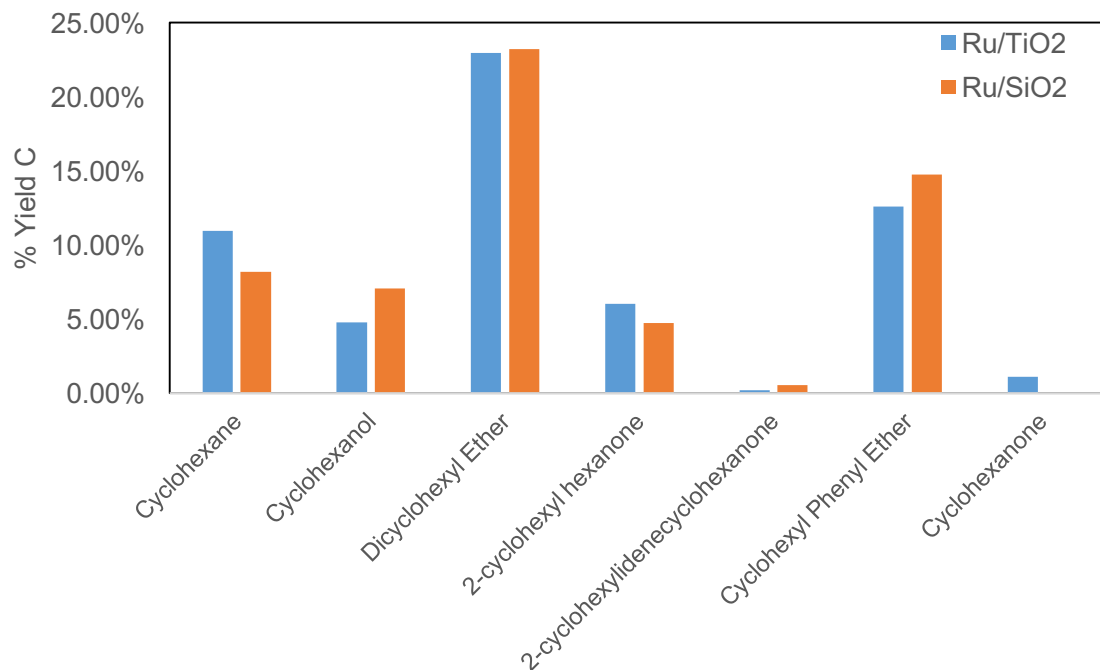


Figure 3.6. Yield of products over Ru/TiO₂ and Ru/SiO₂.

Carbon-carbon formation products are the results of catalysts with the presence of acidity. When metal is not fully reduced during the *in situ* reduction and still in the metal oxide form, the catalyst possesses an acidic property and the tendency to catalyze a carbon-carbon coupling reaction. When the catalyst was reduced for 12 hours to ensure that ruthenium is fully reduced to metallic ruthenium, the bicyclic molecules still appeared after the reaction. This suggests that three hours of reduction is sufficient to reduce RuO to metallic ruthenium and it is confirmed from TPR that the top peak of ruthenium starts is at 172°C. It is worth to mention that in a high pressure of hydrogen, the reduction peak should also be shifted to a lower temperature. This suggests that it should be other acid characteristic of the metal that catalyzed carbon-carbon formation.

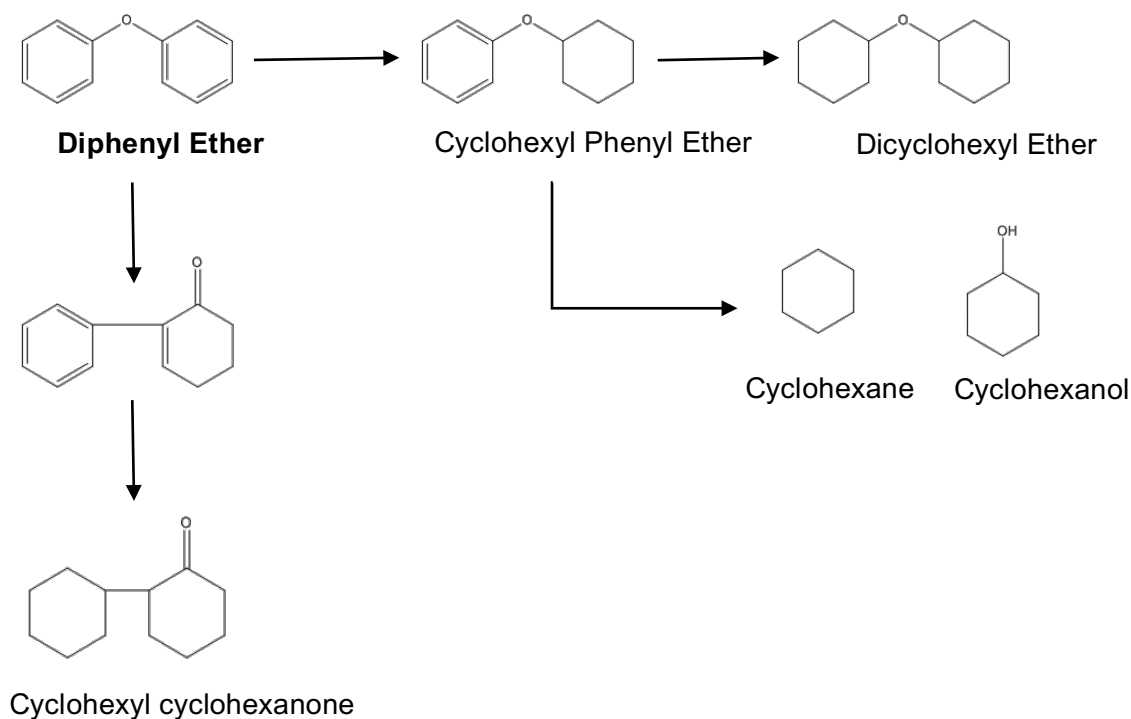


Figure 3.7. Reaction pathway of diphenyl ether over Ru/SiO₂.

The results in Table 3.2 compares two ruthenium catalysts that were prepared by different precursors. One was prepared by ruthenium(III) chloride while the second catalyst was prepared by ruthenium(III) nitrosyl nitrate precursor. The result shows that the catalyst prepared by ruthenium(III) nitrosyl nitrate did not have carbon-carbon molecules. Hence, the catalyst should not contain acidity and ruthenium oxide is fully reduced to metallic ruthenium. As seen from a pyridine-FTIR experiment that Ru/SiO₂ prepared by ruthenium(III) chloride contains Lewis acidity and therefore could catalyze C-C formation reaction. Hence, we observed 2-cyclohexyl cyclohexanone and a trace of 2-cyclohexylidenecyclohexanone in this catalyst. Lewis acid sites could probably be due to the chloride ions residue after calcination at 500°C. Therefore, when the catalyst was reduced in situ before the reaction, ruthenium ions were not reduced to metallic ruthenium. Hence, ruthenium ion that bond to chloride acts as Lewis acid site.

Table 3.2. Yield of products over two different ruthenium precursor: RuCl₃ and Ru(NO)(NO₃)₃.

Products	Yield (%)	
	RuCl ₃	Ru(NO)(NO ₃) ₃
Cyclohexane	11	17
Cyclohexanol	10	7
Cyclohexyl Ether	32	70
2-Cyclohexyl Cyclohexanone	6	0
2-Cyclohexylidenecyclohexanone	1	0
Cyclohexyl Phenyl Ether	20	0

Three possible pathways were postulated for the formation of 2-cyclohexyl cyclohexane.

1. The reaction occurs via the partial hydrogenation of aryl ring. As one of the rings is partially hydrogenated, carbon-carbon bond forms and thus break the C-O bond.

2. Both the aryl rings are hydrogenated forming cyclohexyl ether first then the C-C bond is formed.

3. The reaction happens via alkylation of phenol and cyclohexene where phenol is the alkylating agent.

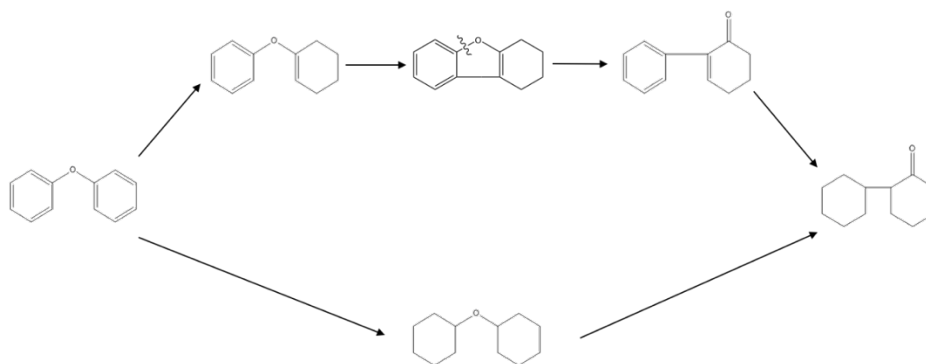


Figure 3.8. Two possible rearrangement pathways to the C-C formation.

To have a better understanding of the reaction pathway of the formation of carbon-carbon products, diphenyl ether was fed in 1% Rh/SiO₂ at 423K. This results in 100 % conversion of diphenyl ether with 65% carbon yield of cyclohexyl ether and the rest are cyclohexane and cyclohexanol. The mixtures were filtered to separate catalyst. By feeding cyclohexyl ether that has both saturated rings, we can differentiate the reaction pathway in possibility one and two. The liquid products mixture was used as the feed in the second reaction with 5% Ru/SiO₂ carrying out at 363K. After 1 hour of reaction, the products show no carbon-carbon bond formation products and thus confirmed that the formation of 2-cyclohexyl cyclohexane from saturated rings is not possible. Therefore, there are only two possibilities that the carbon-carbon products are found in the acid environment are through the rearrangement of the partially hydrogenated ring or via the alkylation of phenol and cyclohexene.

Wagholigar S.G. et al., observed Claisen rearrangement at 353 K using zeolites. Under Bronsted-catalyzed reaction, the main product of allyl phenyl ether reaction is allylphenol. The reaction is catalyzed by the acid centers of zeolites by protonating the ether followed by intramolecular rearrangement [45]. The plausible mechanism of the

diphenyl ether to C-C molecule is via the rearrangement starting with a partial hydrogenation on one of the rings followed by intramolecular rearrangement. Ether carbon on the aromatic bonds to the allyl carbon forming an unstable five-membered ring. C-O ether bond on the aromatic is cleaved and further hydrogenate to form 2-cyclohexyl cyclohexane.

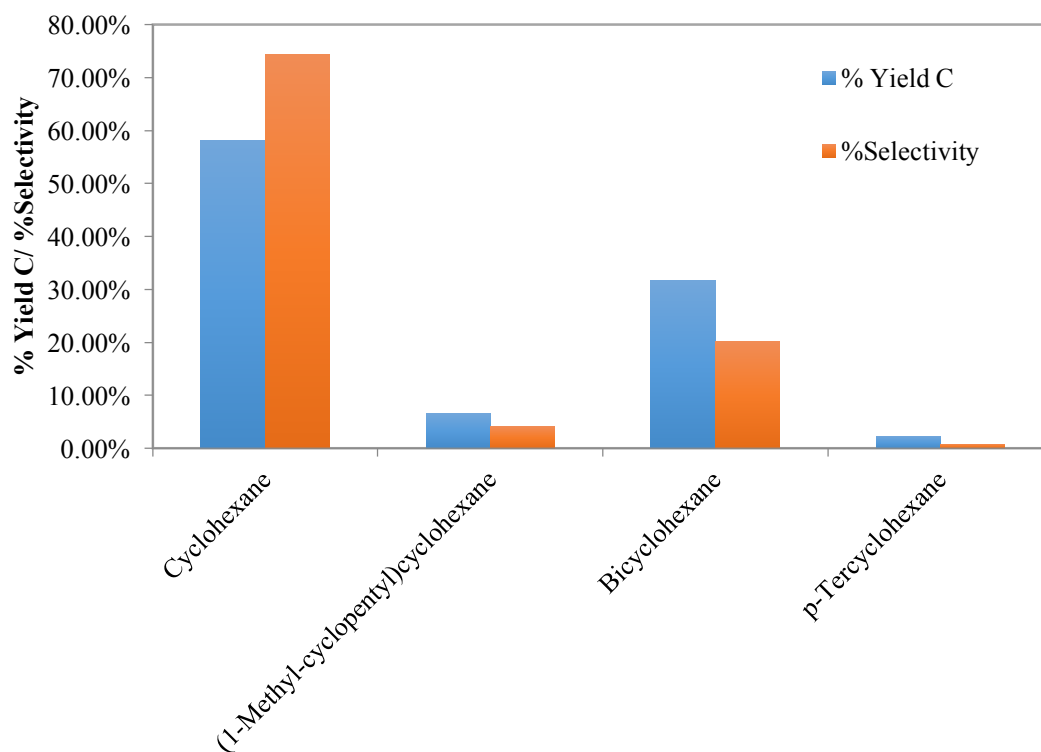


Figure 3.9. Yield and selectivity of products over 5%PdOTS/HY.

Figure 3.9 shows yield and selectivity of the products from diphenyl ether reaction with 5% PdOTS/HY. The catalyst possesses both metal site and acid site. The reaction was performed at 523 K. The major product is cyclohexane and other deoxygenated carbon-carbon formation products as minor products. The yield of carbon-carbon molecules is as high as 35%. Among the carbon-carbon molecules products, 85% of the

yield is bicyclohexane, 10 % is (1-methyl-cyclopentyl)cyclohexane and the rest is tercyclohexane. No phenol or cyclohexanol was observed in the products.

3.4 Conclusions

In diphenyl ether with Ru/SiO₂ prepared by ruthenium(III) chloride that possesses Lewis acid characters, hydrogenation, carbon-carbon rearrangement and alkylation proceed together. Cyclohexyl phenyl ether is the primary product while at longer reaction time cyclohexyl ether becomes the dominant product. Cyclohexane and cyclohexanol reached a plateau after 1 hour. This suggests that hydrogenation of the ring is faster than C-O bond cleavage. When the catalyst possesses acidity character, carbon-carbon bond formation via intramolecular rearrangement results in 2-cyclohexyl cyclohexanone.

Chapter 4. C-O Bond Cleavage of Diphenyl Ether over PdOTS/HY

The experimental data in this chapter was performed by Cristiane Scaldaferrri at the University of Oklahoma. My contribution to this study is the kinetic fittings in section 4.3.4 and BET analysis of the catalysts performed at the University of Oklahoma. I also mentored and played an important role in contributing to the discussions of this work.

This chapter is a (to be published) Cristiane Scaldaferrri, Puridej Warakunwit, Vanya Pasa and Daniel Resasco's paper.

4.1 Introduction

The utilization of lignocellulosic biomass as a renewable energy has gained much attention to reduce the dependence on the fossil fuels consumption and reduce the carbon footprint from the greenhouse effect. Biomass depolymerization has been studied extensively over the past decades, one specifically is the lignin depolymerization. Biomass composes of 13-30 % by weight of lignin. Lignin is a big chain of polymers that are linked by different linkages of C-O and C-C bonds. The most abundant linkage in the lignin is β -O-4 that may contain up to 40% and it has been the targeted ether bond in many studies. 4-O-5, on the other hand, may only have up to 5% in the lignin but it has one of the strongest bond dissociation energy (BDE) of 314 kJ mol^{-1} . [46]–[49]

There are many challenges to fully unlock the lignin's potential. The most challenge is since lignin contains many C-O-C ether bonds that need to selectively cleave to monomers. Extensive studies on hydrodeoxygenation of lignin-derived molecules have been conducted. Such examples are metal triflate and Ru-based solid catalyst [50], Ru-Ni supported onto nitrogen-doped activated carbon [51], m-cresol on Pt/SiO₂ [52] or the bimetallic catalysts over gamma-alumina [53]–[55].

Homogeneous and heterogeneous catalytic systems have been studied for the ether bond cleavage in the literature. Ni/SiO₂ under mild condition was studied by J. He et al. It was observed that the C-O bond of diphenyl ether is cleaved by both hydrogenolysis and hydrolysis in parallel. The rate of direct hydrogenation of the ring was slow. While on di-p-tolyl ether, which has methyl groups, hydrogenolysis is the dominant pathway [36]. Similar to this study, X. Wang et al. have shown that at high pressure of hydrogen (5MP) nickel catalysts such as Raney Ni and Ni/Al₂O₃ yielded up to 50% of cyclohexyl ether, the result of the hydrogenation of the rings. They demonstrated that Ni/Al-SBA-15 fully converted diphenyl ether into cyclohexane and therefore is an active catalyst for hydrodeoxygenation [37].

H. Wu et al. have shown that Ru/C could efficiently cleave diphenyl ether via a transfer hydrogenolytic route using isopropanol as the hydrogen source. They have stated that the cleavage of the 4-O-5 ether bond occurred through both the direct cleave of the aromatic ether bonds or the intermediate cyclohexyl phenyl ether [56]. The cleavage of the ether bond could result in cyclohexene and phenol which would be beneficial to the alkylation for carbon-carbon bond formation.

From the previous chapter on the study of the hydrogenation of diphenyl ether over Ru/SiO₂, we observed that an oxophilic ruthenium metal is good at C-O bond cleavage and the catalyst that was prepared by ruthenium(III) chloride precursor also has residue chloride ions after calcination. These resulting ions cause this metal catalyst to possess Lewis acidity, which catalyzes the carbon-carbon bond formation. From carbon-carbon formation, either by intramolecular rearrangement or the C-O bond cleavage followed by

the alkylation, the C-12 oxygenated molecules can be deoxygenated or hydrogenation to a saturated bicyclic molecule that is used for transportation fuels.

To further investigate the carbon-carbon bond formation, a metal-acid bifunctionality catalyst will be explored in this chapter. The balance between hydrogenation and C-O bond cleavage activities depend on the nature and the availability of metal and acid active sites. As previously stated that the order of the oxophilicity of the metal is $\text{Pt} < \text{Pd} < \text{Rh} < \text{Ru} < \text{Fe}$ [41], [57]. Therefore, the metal Pd with a weak oxophilicity was chosen for this study to allow the hydrogenation of the ring. For the acid functionality, zeolite Y that is known for a good Bronsted acid-catalyzed reaction is chosen for this study.

4.2 Experiments

Zeolite HY (Zeolyst, CBV 760, Si/Al =30) and HiSil SiO₂ were used as provided. Palladium (II) nitrate hydrate was used as the precursor for incipient wetness impregnation. In a typical preparation, palladium precursor was dissolved in the deionized water then the metal precursor solution was added dropwise and stirred. After the impregnation, the catalyst was dried overnight at 80°C in the oven. The catalyst was calcined in air at 400°C. Prior to functionalize the catalyst with octadecyltrichlorosilane (OTS), the metal-loaded zeolite was sonicated in toluene for 1 hour with a ratio of 20 mL of toluene per gram of zeolite. Then, the dispersed zeolite suspension was added to the silylating agent solution. The suspension was stirred for 12 hours at room temperature before the resulting catalyst was filtered and washed with excess ethanol. The catalyst was dried at 100°C overnight.

The BET surface area of the catalyst was measured by N₂ physisorption on a Micrometrics ASAP 2020. The catalyst was degassed for 6 hours at 200°C prior to the analysis.

All experiments were carried out in 50-mL Parr Reactor. In a typical experiment, the catalyst with 20 mL of decalin (Sigma Aldrich, 99%) was loaded into the reactor. The reactor was purged with N₂ three times, then pressurized with H₂ to 200 psi to reduce the catalyst. After the reduction, the system was cooled down to 70°C to inject diphenyl ether (Sigma Aldrich, ≥99%) diluted in decalin from a pressurized feeding cylinder then pressurized the reactor to 700 psi of H₂. The zero reaction time started once the temperature reached the set temperature. After the reaction, the reaction was stopped by a rapid cool down with ice bath. The catalyst was removed via filtration. Analyzes were done using a Hewlett Packard 6890 GC-FID equipped with DB-1701 column (60 m x 0.25 mm x 0.25 μm) for quantification, while a Shimadzu QP2010 GC-MS equipped with ZB-1701 column (60 m x 0.25 mm x 0.25 μm) was used for products identification.

4.3 Results and Discussion

4.3.1 Role of Hydrophobicity

It is well known that zeolite is susceptible to hot liquid water. When the zeolite is exposed to liquid water, it can collapse the pore of the zeolites. In order to maximize the stability and activity of the catalyst, the experiments were chosen to perform in the organic phase and used functionalized zeolite that had shown to resist the liquid water [58], [59]. Table 4.1 shows that both Pd/HY and PdOTS/HY reactions in decalin (an organic solvent), the carbon balances are comparable. However, when the reactions were

carried out in a biphasic system with water and decalin, the activity of Pd/HY is about 9 times lower than PdOTS/HY while carbon balances are at reasonable level. Therefore, in this study PdOTS/HY were used to study the carbon-carbon bond formation in diphenyl ether reaction.

Table 4.1. Conversion and carbon balance of PdOTS/HY and Pd/HY in organic phase and biphasic system.

Catalyst	Conversion in organic phase (%)	Conversion in a biphasic system (%)	Carbon balance in organic phase (%)	Carbon balance in a biphasic system (%)
PdOTS/HY	98	47	74	88
Pd/HY	75	5	73	96

To identify the primary and secondary products, the product distribution as the function of the extent reaction in the batch reactor is studied. Since deactivation was observed as seen in Table 4.1, the reaction time was fixed at 1 hour over different masses of the catalyst. From Figure 4.1, at low conversion, the major products are cyclohexane, cyclohexanone, and phenol. A trace amount of benzene and cyclohexyl phenyl ether was observed. Traces of C-C molecules, namely, 1,1-bicyclohexyl and 1,1-bicyclohexyl-2-one were seen. As the catalyst mass increased both benzene and phenol disappeared. The yield of carbon-carbon molecule increased. Cyclohexanone yield reaches a plateau at 30 mg of catalyst while the yield of cyclohexane keeps increasing. This shows that the yield

of cyclohexane was not only coming from diphenyl ether directly but also from hydrogenation of cyclohexanone to cyclohexanol then deoxygenate to cyclohexane. At 98% conversion, the yield of the carbon-carbon molecules was as high as 25.1%. Among 25% yield of the carbon-carbon molecules, 21.3% was 1,1-bicyclohexyl-2-one, 1.9% of 1,1-bicyclohexyl and a trace of 1,1-bicyclohexyl-4-one.

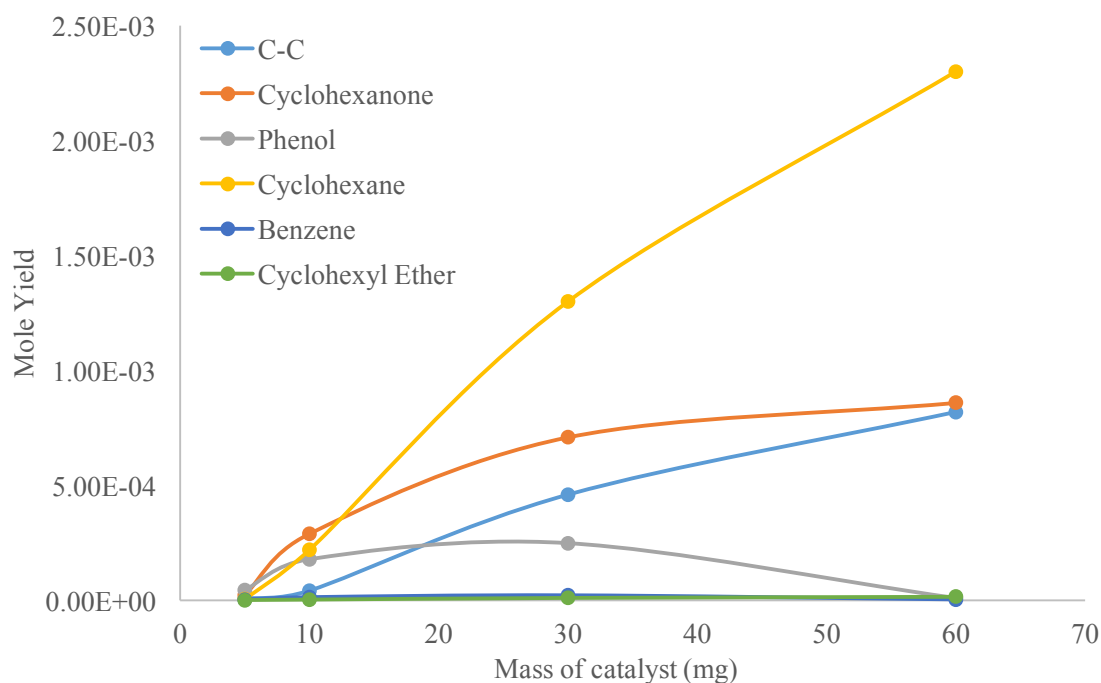


Figure 4.1. Mole of products over different mass of catalyst.

From the products distribution, it shows that once one of the aromatic is hydrogenate to cyclohexyl phenyl ether, the C-O bond is cleaved to benzene and cyclohexanone or phenol and cyclohexane. The favorable pathway to C-O bond cleavage will be discussed later. Second hydrogenation of the ring obtains cyclohexyl ether but it was not observed in any reactions.

4.3.2 Role of metal and acid sites

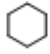

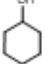

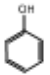
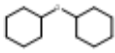
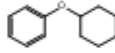
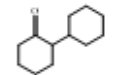
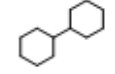
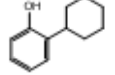
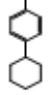
Catalysts	OTS/HY	2%Pd/SiO ₂	1%PdOTS/HY
Products yield (%)	0	37	58
C balance (%)	90	92	88

PdOTS/HY has both metal site and the Bronsted acid sites in the zeolites. To understand the role of each function, experiments on only acid sites, OTS/HY, and metal sites, Pd/SiO₂, were carried out. All the reactions were done under the same reaction conditions.

Table 4.2. Products yield and carbon balance of diphenyl ether reaction over OTS/HY, 2% Pd/SiO₂ and 1% PdOTS/HY.

From Table 4.2, we can see that OTS/HY with only the acid sites, there was no conversion of diphenyl ether. This says that without the metal site, no hydrogenation happens, consequently no C-O bond cleavages. While on Pd/SiO₂, the conversion was 37%. Since it only contains metal site, the reaction precludes carbon-carbon formation molecules and suppress C-O cleavage. The products account for a high selectivity of cyclohexyl phenyl ether and cyclohexyl ether was observed with 8.8% of selectivity. Pd/SiO₂ was able to cleave C-O bond which resulted in traces of cyclohexane, cyclohexanol, benzene, and phenol. As compared to PdOTS/HY, the selectivity shifted to C-O bond cleavage products and carbon-carbon molecules formation. Herein, we can conclude that PdOTS/HY provides both metal functionality to hydrogenate and acidity to form carbon-carbon molecule.

Table 4.3. Products yield and selectivity of diphenyl ether over Pd/SiO₂ and PdOTS/HY

Products	Pd/SiO ₂		PdOTS/HY	
	Selectivity (%)	Yield (%)	Selectivity (%)	Yield (%)
	1.3	0.3	46.6	18.1
	4.7	0.9	1.2	0.5
	2.5	0.5	0.3	0.2
	9.6	1.8	26.2	10.2
	0.5	0.1	9	13
	8.8	3.3	0	0
	72.3	27.6	0.5	0.4
	0	0	12.7	10
	0	0	1.3	1
	0	0	1.9	1.5
	0	0	0.6	0.5

4.3.3 C-O Cleavage

As mentioned earlier, no cyclohexyl ether had been detected in any reactions. The hypothesis is when one of the aromatic rings on diphenyl ether is hydrogenated to cyclohexyl phenyl ether, the C-O bond is cleaved to monomers.

Two reasons that no C-O bond cleavage happens on diphenyl ether.


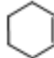

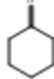
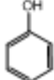
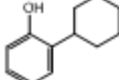

1. The protonation of oxygen on the ether bond would decrease the bond distance between $C_{\text{aromatic}}-O_{\text{ether}}$, therefore, requires a high activation energy.
2. Even if the C-O bond cleavage happens, phenyl cation is thermodynamically unstable. The phenyl cation carries a positive charge in sp^2 orbital that cannot be stabilized by resonance.

Therefore, a more favorable pathway for C-O bond cleavage of diphenyl ether is via the ring hydrogenation followed by the protonation of the oxygen on the ether bond. Next, alpha-hydrogen on cyclohexyl deprotonates and then cleaves C-O bond resulting in phenol and cyclohexene.

Table 4 summarizes the products distribution from C-O bond cleavage from cyclohexyl phenyl ether. In order to understand C-O bond cleavage, the reactant was studied over OTS/HY, which only has acid sites, to minimize the ring hydrogenation. There are two possibilities to cleave C-O bond on the ether linkage. One is at the carbon of the aromatic ring which results in benzene and cyclohexanone. Another possibility is by cleaving at the carbon of the cyclic saturated hydrocarbon and will result in cyclohexane and phenol. The result shows that it is more favorable to cleave the C-O bond on the carbon of the cyclic hydrocarbon as confirmed by the selectivity of phenol

and cyclohexene of 43% and 46%, respectively and less than 5% of selectivity to benzene and cyclohexanone. Other than the mentioned monomers, carbon-carbon molecules were also observed.

Table 4.4. Products yield and selectivity of cyclohexyl phenyl ether over PdOTS/HY.

Products	Selectivity (%)	Yield (%)
	4.0	0.8
	46.2	8.9
	0.3	0.1
	4.4	0.8
	43.1	8.3
	1.8	0.7
	0.3	0.1

The formation of carbon-carbon molecules has two reaction pathway. The first pathway is by alkylation as observed by Anaya, F. et al [60]. Alkylation happens after cyclohexyl phenyl ether is cleaved to phenol and cyclohexene. The second pathway is a

direct rearrangement of cyclohexyl phenyl ether. However, both pathways result in the same ortho products, 2-cyclohexyl phenol (A) and 1,1-bicyclohexyl-2-one (B).

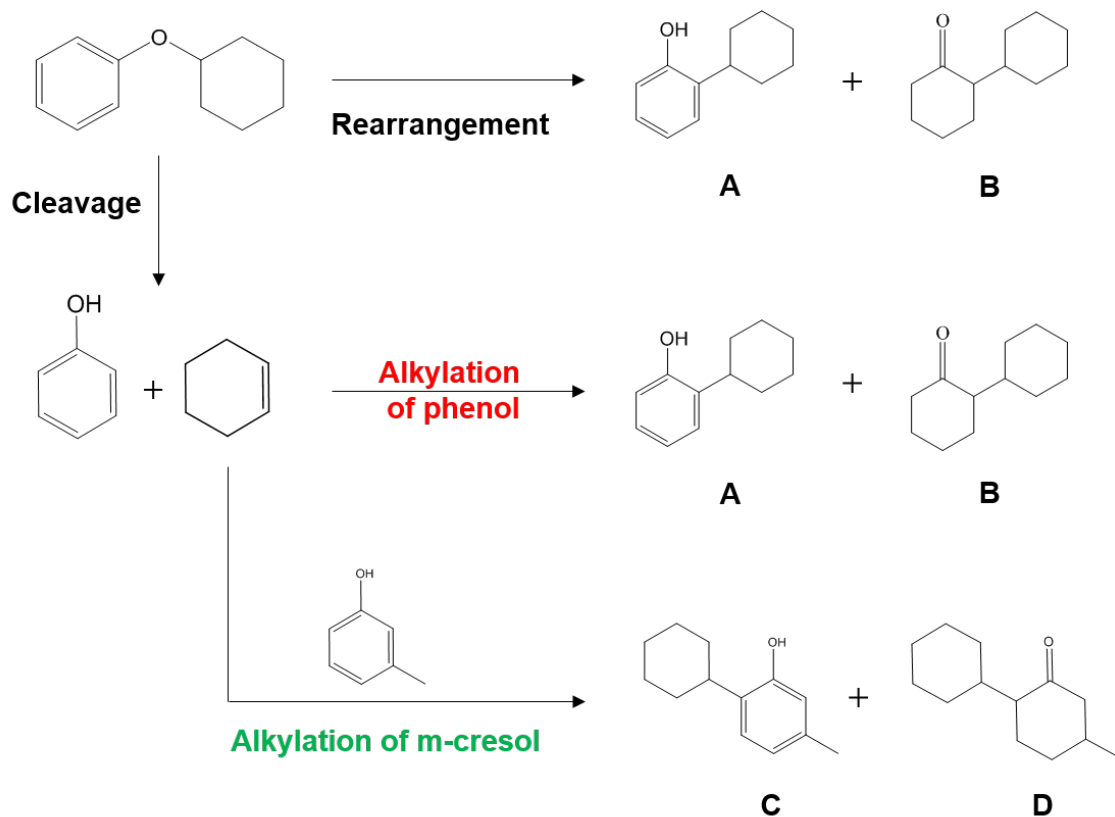


Figure 4.2. Reaction pathways of rearrangement, alkylation of phenol and cyclohexene and alkylation of phenol and m-cresol.

To distinguish the two carbon-carbon formation pathways, another substrate is needed. M-cresol, which has a methyl group attached to the aromatic ring, was co-fed with and diphenyl ether. As seen from Figure 4.2, when m-cresol alkylated with cyclohexene, the most favorable position is still at the ortho position, resulted in 2-cyclohexyl-5-methylphenol (C) and 4-methyl-(1,1-bicyclohexyl)-2-one (D) forms. But, the products resulting from rearrangement and alkylation are differentiable. Table 4.5 compares the molar ratio of the products (C+D)/(A+B) as the molar ratio of m-cresol/DPE

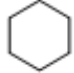
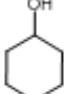
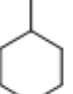
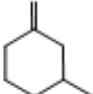
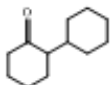
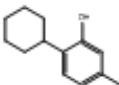
increases. When the molar ratio of m-cresol-to-DPE increased from 0 to 1, the molar ratio of (C+D)/(A+B) also increased from 0 to 2.12. This trend shows that alkylation pathway is more favorable than the ring rearrangement.

Table 4.5. Molar ratio of C-C products from alkylation of m-cresol/C-C products from rearrangement or alkylation of phenol.

Molar ratio cresol/DPE	DPE conversion (%)	DPE C balance (%)	Cresol conversion (%)	Cresol C balance (%)	% Alkylated products yield from phenol (A+B)	% Alkylated products yield from cresol (C+D)	Molar ratio (C+D)/(A+B)
0	17	93	-	-	4.80	0	0
0.25	24	87	71	89	3	0.88	0.30
0.5	23	92	56	83	1.15	0.96	0.76
1	21	90	38	88	0.41	1.10	2.12

Even though that the major products from hydrogenation of m-cresol and cyclohexanone are cyclohexane and methyl-cyclohexanone but Table 4.6 shows that alkylation of m-cresol and cyclohexanone results in two carbon-carbon coupling products which are 1,1-bicyclohexyl-2-one that dominates over 2-cyclohexyl-5-methylphenol. From reaction pathway in Figure 4.3, phenol hydrogenates to cyclohexanone which could self-condensate to 1,1-bicyclohexyl-2-one (B).

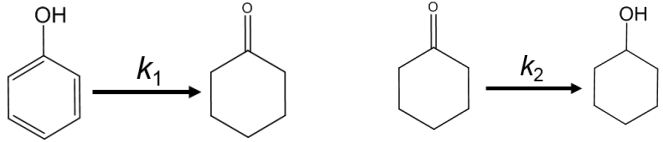
Table 4.6. Products selectivity of alkylation m-cresol and cyclohexanone.

Products						
Selectivity, %	49.3	20.8	2.9	20.6	5.4	1.0

4.3.4 Kinetic fitting of hydrogenation of phenol and hydrogenation of cyclohexanone.

As mentioned earlier that the maximum yield of alkylating products is 23% while the yield of cyclohexane is tripled. From the reaction pathway scheme, in order to maximize alkylation is to maximize a pool of cyclohexene that serves as the alkylating agent, but the earlier results suggest otherwise. Once cyclohexene formed, it hydrogenated to cyclohexane much faster than alkylated with phenol.

Table 4.7. Rate constants of hydrogenation of phenol (k_1) and hydrogenation of cyclohexanone (k_2).

		
Rate constant ($\text{g}^{-1}\text{hr}^{-1}$)	41	6

How fast phenol hydrodeoxygenate to cyclohexene is also another factor. In a batch reactor, the rate of reaction can be derived as followed

$$r_a = -kC_a W$$

$$C_{a_0} = C_a \exp^{-kWt}$$

$$\frac{dC_a}{dW} = kC_a t$$

where k = rate constant

W = mass of catalyst (gram)

t = time (hour)

Therefore, by feeding phenol or cyclohexanone at different mass of catalyst and fix the time at 1 hour, we can fit the data to the below kinetic modeling in Excel.

For hydrogenation of phenol to cyclohexanone,

$$dC_{\text{phe}}/dW = -k_1 C_{\text{phe}} t$$

$$dC_{\text{con}}/dW = k_1 C_{\text{phe}} t$$

For hydrogenation of cyclohexanone to cyclohexanol,

$$dC_{\text{one}}/dW = -k_2 C_{\text{one}} t$$

$$dC_{\text{col}}/dW = k_2 C_{\text{one}} t$$

Fitting hydrogenation of phenol and hydrogenation of cyclohexanone at different conversion with kinetic modeling, the rate constant, k_1 , for hydrogenation of phenol was equaled to $41 \text{ g}^{-1}\text{hr}^{-1}$, while k_2 , the rate constant for hydrogenation of cyclohexanone was $6 \text{ g}^{-1}\text{hr}^{-1}$. The rate constant of hydrogenation of phenol to cyclohexanone is almost 7 times higher than that of hydrogenation of cyclohexanone to cyclohexanol. This entails that the reaction is limited by cyclohexanone hydrogenation and cyclohexanone has a stronger adsorption on Pd. Therefore, hydrogenation of cyclohexanone to cyclohexanol is a rate-limiting step to form cyclohexene. Nevertheless, this also explains that in diphenyl ether reactions with Pd/OTSHY, no cyclohexene was detected.

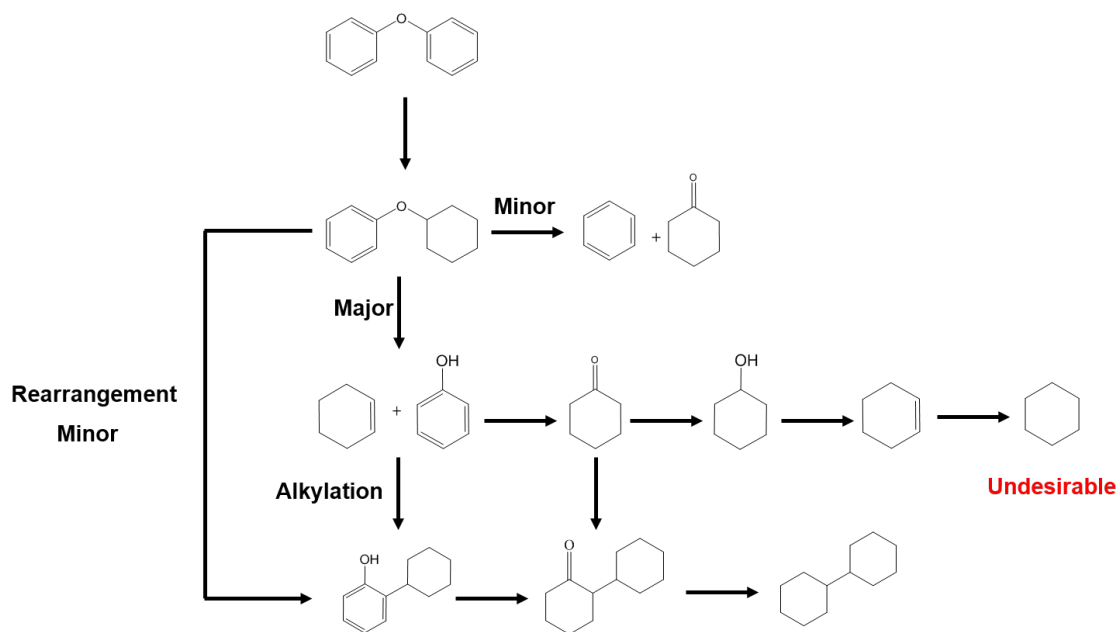


Figure 4.3. Reaction pathways of diphenyl ether over PdOTS/HY

4.3.5 Metals and Acid Sites Balance

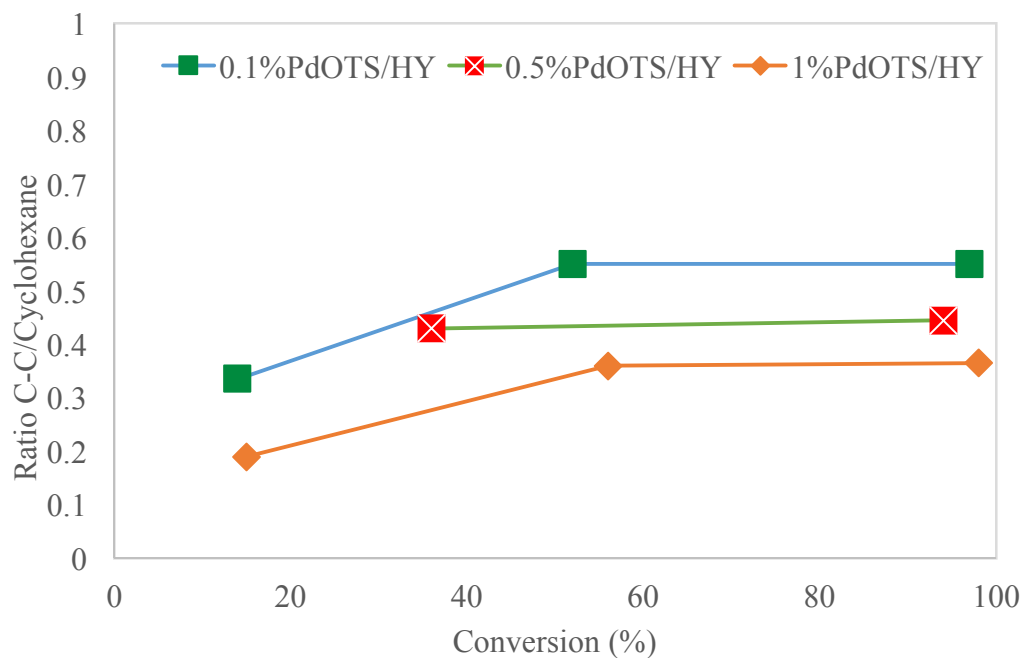


Figure 4.4. Ratio of a total mole of C-C/Cyclohexane over different conversion.

To evaluate the role of metal and acid sites, the ratio of carbon-carbon products to cyclohexane were evaluated in the different loading of Pd. Figures 4.4 reviews the effect of palladium loading from 0.1% to 1% on zeolites on the ratio of carbon-carbon products/cyclohexane. The trend of the ratio shows that at a lower loading of palladium, a higher ratio of C-C to cyclohexane was observed. The ratio of C-C to cyclohexane of 1% PdOTS/HY was 0.2 at 20% conversion and reached a maximum at 0.3 at 60% conversion. As the loading of palladium decreased to 0.1%, the ratio increased to 0.55. With smaller loading of palladium, the number of acid sites per gram should be higher and so favor the alkylation of the intermediates. These trends show that by controlling the metal and acid sites, one could optimize the alkylated products.

4.4 Conclusions

The reaction of diphenyl ether over PdOTS/HY was studied in the liquid phase. The results show that the carbon-carbon formation happened through alkylation over rearrangement. C-O bond is cleaved once one of the rings in diphenyl ether is hydrogenated (cyclohexyl phenyl ether) resulting in cyclohexene and phenol. These products further alkylate to form C-C coupling molecules. Formation of C-C molecules was limited by hydrogenation of cyclohexanone to cyclohexanol that further hydrogenate to cyclohexene.

Future Directions and Recommendations

From the study of lignin depolymerization, we have observed that methanol and ethanol are excellent solvents to solubilize the lignin. From the ethanolysis of Red Oak biomass, ethanol was able to isolate the lignin from cellulose and hemicellulose during the reaction and allowed the cellulose and hemicellulose to remain intact in the biomass. This result has shown a great potential to develop the strategy to maximize the utilization of biomass. As proposed earlier in Chapter 2, in order to increase the potential of biomass to biofuels, after ethanolysis of biomass, the non-pyrolytic bio-oil should be treated to remove heavy macromolecules. This is evidenced by no increase in the yield of monomers even though that more lignin was solubilized with the addition of catalyst. By trapping the heavy oligomers on a support material, it can be treated by thermal pyrolysis to produce valuable chemicals. Now that the non-pyrolytic bio-oil is clean, it can be upgraded with the potential catalyst.

One of the example of the changing in the direction of tackling and utilize the biomass is a publication from D. M. Alonso et al. The group has highlighted the importance of biofuels being cost- and performance- competitive with the fossil fuels. They have proposed a strategy that can preserve the value of all three components in the biomass and use 80% of the biomass to high-value products. The process converts cellulose to dissolving pulp for textile fibers. Furfural is derived from hemicellulose while lignin is converted into carbon products such as carbon foam and battery anodes. The process is possible by using γ -valerolactone (GVL) [61].

From the study in Chapter 3 and Chapter 4, we observed that 4-O-5 ether linkage in lignin has a high potential to produce C12 molecules which can be used for transportation fuels. Even though that the % content of 4-O-5 is not as high as other linkage such as β -O-4 but it is as important. Eventually more of 4-O-5 and β - β linkages are needed to be studied and understood as more of these bonds would be found after the repolymerization during the deconstruction of the polymers chain. From our study, we have seen that ruthenium is a good metal for C-O bond cleavage due to its oxophilicity, therefore, it could potentially be used for the lignin depolymerization to break the ether bonds. Diphenyl Ether over PdOTS/HY has also shown that with a good balance of metal and acidity, it was able to cleave C-O bond as well as forming carbon-carbon bond through alkylation.

From the model compound study, the depolymerization of lignin using different bifunctional catalyst could also be a good potential to enhance the yield of the monomers. However, it is important that the acid support must be a non-porous to avoid the plugging of the pores from heavy molecules.

References

- [1] D. M. Alonso, S. G. Wettstein, and J. A. Dumesic, "Bimetallic catalysts for upgrading of biomass to fuels and chemicals," *Chem. Soc. Rev.*, vol. 41, no. 24, pp. 8075–8098, 2012.
- [2] T. V Bui, S. Crossley, and D. E. Resasco, "C – C Coupling for Biomass-Derived Furanics Upgrading to," 2016.
- [3] D. E. Resasco and S. P. Crossley, "Implementation of concepts derived from model compound studies in the separation and conversion of bio-oil to fuel," *Catal. Today*, vol. 257, no. P2, pp. 185–199, 2015.
- [4] P. Ferrini and R. Rinaldi, "Catalytic biorefining of plant biomass to non-pyrolytic lignin bio-oil and carbohydrates through hydrogen transfer reactions," *Angew. Chemie - Int. Ed.*, vol. 53, no. 33, pp. 8634–8639, 2014.
- [5] G. W. Huber, S. Iborra, and A. Corma, "Synthesis of transportation fuels from biomass: Chemistry, catalysts, and engineering," *Chem. Rev.*, vol. 106, no. 9, pp. 4044–4098, 2006.
- [6] R. Rinaldi *et al.*, "Paving the Way for Lignin Valorisation: Recent Advances in Bioengineering, Biorefining and Catalysis," *Angew. Chemie - Int. Ed.*, vol. 55, no. 29, pp. 8164–8215, 2016.
- [7] Z. Sun, B. Fridrich, A. De Santi, S. Elangovan, and K. Barta, "Bright Side of Lignin Depolymerization: Toward New Platform Chemicals," *Chem. Rev.*, vol. 118, no. 2, pp. 614–678, 2018.
- [8] J. E. Holladay, J. F. White, J. J. Bozell, and D. Johnson, "Top Value-Added Chemicals from Biomass Volume II - Results of Screening for Potential Candidates from Biorefinery Lignin," *Pacific Northwest Natl. Lab.*, vol. II, no. October, p. 87, 2007.
- [9] J. A. Schmidt, C. R. C. P. Taylor, J. Ralph, and L. L. Landucci, "Lignin and Lignans; Advances in Chemistry," pp. 137–234, 2010.
- [10] G. G. D. Dimmel, "Lignin and Lignans: Advances in Chemistry (Eds.: C. Heitner, D. R. Dimmel, J. A. Schmidt), CRC Press, Boca Raton, 2010, pp. 349–391," pp. 349–391, 2010.
- [11] B. M. G. Gellerstedt, E. L. Lindfors, C. Lapierre, "Structural changes in lignin during kraft cooking Part 4. Phenolic hydroxyl groups in wood and kraft pulps," *Sven. Papperstidning-Nordisk Cellul.*, vol. 87, pp. R61–R67, 1984.
- [12] M. R. Sturgeon *et al.*, "Lignin depolymerisation by nickel supported layered-double hydroxide catalysts," *Green Chem.*, vol. 16, no. 2, pp. 824–835, 2014.

- [13] K. Zhang, Z. Pei, and D. Wang, "Organic solvent pretreatment of lignocellulosic biomass for biofuels and biochemicals: A review," *Bioresour. Technol.*, vol. 199, pp. 21–33, 2016.
- [14] X. Wang and R. Rinaldi, "Solvent effects on the hydrogenolysis of diphenyl ether with raney nickel and their implications for the conversion of lignin," *ChemSusChem*, vol. 5, no. 8, pp. 1455–1466, 2012.
- [15] J. S. Luterbacher, A. Azarpira, A. H. Motagamwala, F. Lu, J. Ralph, and J. A. Dumesic, "Lignin monomer production integrated into the γ -valerolactone sugar platform," *Energy Environ. Sci.*, vol. 8, no. 9, pp. 2657–2663, 2015.
- [16] X. Huang, T. I. Korányi, M. D. Boot, and E. J. M. Hensen, "Ethanol as capping agent and formaldehyde scavenger for efficient depolymerization of lignin to aromatics," *Green Chem.*, vol. 17, no. 11, pp. 4941–4950, 2015.
- [17] X. Huang, T. I. Korányi, M. D. Boot, and E. J. M. Hensen, "Catalytic depolymerization of lignin in supercritical ethanol," *ChemSusChem*, vol. 7, no. 8, pp. 2276–2288, 2014.
- [18] J. Y. Kim, J. Park, U. J. Kim, and J. W. Choi, "Conversion of Lignin to Phenol-Rich Oil Fraction under Supercritical Alcohols in the Presence of Metal Catalysts," *Energy and Fuels*, vol. 29, no. 8, pp. 5154–5163, 2015.
- [19] S. Van den Bosch, W. Schutyser, S.-F. Koelewijn, T. Renders, C. M. Courtin, and B. F. Sels, "Tuning the lignin oil OH-content with Ru and Pd catalysts during lignin hydrogenolysis on birch wood," *Chem. Commun.*, vol. 51, no. 67, pp. 13158–13161, 2015.
- [20] N. Yan, C. Zhao, P. J. Dyson, C. Wang, L. T. Liu, and Y. Kou, "Selective degradation of wood lignin over noble-metal catalysts in a two-step process," *ChemSusChem*, vol. 1, no. 7, pp. 626–629, 2008.
- [21] R. Ma, W. Hao, X. Ma, Y. Tian, and Y. Li, "Catalytic ethanolysis of kraft lignin into high-value small-molecular chemicals over a nanostructured α -molybdenum carbide catalyst," *Angew. Chemie - Int. Ed.*, vol. 53, no. 28, pp. 7310–7315, 2014.
- [22] C. R. Kumar *et al.*, "Solvent free depolymerization of Kraft lignin to alkyl-phenolics using supported NiMo and CoMo catalysts," *Green Chem.*, vol. 17, no. 11, pp. 4921–4930, 2015.
- [23] A. K. Deepa and P. L. Dhepe, "Lignin Depolymerization into Aromatic Monomers over Solid Acid Catalysts," *ACS Catal.*, vol. 5, no. 1, pp. 365–379, 2015.

- [24] T. Renders *et al.*, “Influence of Acidic (H₃PO₄) and Alkaline (NaOH) Additives on the Catalytic Reductive Fractionation of Lignocellulose,” *ACS Catal.*, vol. 6, no. 3, pp. 2055–2066, 2016.
- [25] E. M. Anderson *et al.*, “Reductive Catalytic Fractionation of Corn Stover Lignin,” *ACS Sustain. Chem. Eng.*, p. acssuschemeng.6b01858, 2016.
- [26] B. Gómez-Monedero, M. Pilar Ruiz, F. Bimbela, and J. Faria, “Selective depolymerization of industrial lignin-containing stillage obtained from cellulosic bioethanol processing,” *Fuel Process. Technol.*, vol. 173, no. January, pp. 165–172, 2018.
- [27] O. Faix, I. Fortmann, J. Bremer, and D. Meier, “Thermal degradation products of wood Gas chromatographic separation and mass spectrometric characterization,” *Holz als Roh- und Werkst.*, vol. 49, pp. 213–219, 1991.
- [28] Sunkyu Park, John O Baker, Michael E Himmel, Philip A Parilla, and David K Johnson, “Cellulose crystallinity index: measurement techniques and their impact on interpreting cellulase performance,” *Biotechnol. Biofuels*, vol. 3, no. 10, pp. 1–10, 2010.
- [29] H. Zhao, J. H. Kwak, Z. Conrad Zhang, H. M. Brown, B. W. Arey, and J. E. Holladay, “Studying cellulose fiber structure by SEM, XRD, NMR and acid hydrolysis,” *Carbohydr. Polym.*, vol. 68, no. 2, pp. 235–241, 2007.
- [30] C. L. Waters, R. R. Janupala, R. G. Mallinson, and L. L. Lobban, “Staged thermal fractionation for segregation of lignin and cellulose pyrolysis products: An experimental study of residence time and temperature effects,” *J. Anal. Appl. Pyrolysis*, vol. 126, no. May, pp. 380–389, 2017.
- [31] J. M. Younker, A. Beste, and A. C. Buchanan, “Computational study of bond dissociation enthalpies for lignin model compounds: β -5 Arylcoumaran,” *Chem. Phys. Lett.*, vol. 545, pp. 100–106, 2012.
- [32] J. Huang, C. Liu, Q. Jin, H. Tong, W. Li, and D. Wu, “Density functional theory study on bond dissociation enthalpies for lignin dimer model compounds,” *J. Renew. Sustain. Energy*, vol. 6, no. 3, 2014.
- [33] J. M. Younker, A. Beste, and A. C. Buchanan, “Computational study of bond dissociation enthalpies for substituted β -O-4 lignin model compounds,” *ChemPhysChem*, vol. 12, no. 18, pp. 3556–3565, 2011.
- [34] S. Jin *et al.*, “Cleavage of lignin-derived 4-O-5 aryl ethers over nickel nanoparticles supported on niobic acid-activated carbon composites,” *Ind. Eng. Chem. Res.*, vol. 54, no. 8, pp. 2302–2310, 2015.

- [35] J. Cornella, C. Zarate, and R. Martin, "Metal-catalyzed activation of ethers via C-O bond cleavage: a new strategy for molecular diversity," *Chem. Soc. Rev.*, vol. 43, no. 23, pp. 8081–8097, 2014.
- [36] J. He, C. Zhao, D. Mei, and J. A. Lercher, "Mechanisms of selective cleavage of C-O bonds in di-aryl ethers in aqueous phase," *J. Catal.*, vol. 309, pp. 280–290, 2014.
- [37] X. Wang and R. Rinaldi, "Bifunctional Ni catalysts for the one-pot conversion of Organosolv lignin into cycloalkanes," *Catal. Today*, vol. 269, pp. 48–55, 2016.
- [38] X. Wang and R. Rinaldi, "Solvent effects on the hydrogenolysis of diphenyl ether with raney nickel and their implications for the conversion of lignin," *ChemSusChem*, vol. 5, no. 8, pp. 1455–1466, 2012.
- [39] J. Greeley and J. K. Nørskov, "A general scheme for the estimation of oxygen binding energies on binary transition metal surface alloys," *Surf. Sci.*, vol. 592, no. 1–3, pp. 104–111, 2005.
- [40] N. Duong, Q. Tan, and D. E. Resasco, "Controlling phenolic hydrodeoxygenation by tailoring metal–O bond strength via specific catalyst metal type and particle size selection," *Comptes Rendus Chim.*, vol. 21, no. 3–4, pp. 155–163, 2018.
- [41] Q. Tan *et al.*, "Mechanistic analysis of the role of metal oxophilicity in the hydrodeoxygenation of anisole," *J. Catal.*, vol. 347, pp. 102–115, 2017.
- [42] V. N. Kalevaru, A. Benhmid, J. Radnik, M. M. Pohl, U. Bentrup, and A. Martin, "Marked influence of support on the catalytic performance of PdSb acetoxylation catalysts: Effects of Pd particle size, valence states, and acidity characteristics," *J. Catal.*, vol. 246, no. 2, pp. 399–412, 2007.
- [43] G. Busca, "The surface acidity of solid oxides and its characterization by IR spectroscopic methods. An attempt at systematization," *Phys. Chem. Chem. Phys.*, vol. 1, no. 5, pp. 723–736, 1999.
- [44] L. Chen, Y. Li, X. Zhang, Q. Zhang, T. Wang, and L. Ma, "Mechanistic insights into the effects of support on the reaction pathway for aqueous-phase hydrogenation of carboxylic acid over the supported Ru catalysts," *Appl. Catal. A Gen.*, vol. 478, pp. 117–128, 2014.
- [45] S. G. Waghlikar, S. Mayadevi, N. E. Jacob, and S. Sivasanker, "Claisen rearrangement of allyl phenyl ether over zeolites beta, mordenite and Y," *Microporous Mesoporous Mater.*, vol. 95, no. 1–3, pp. 8–16, 2006.
- [46] J. J. Zhang *et al.*, "Pyrolysis mechanism of a β -O-4 type lignin dimer model compound: A joint theoretical and experimental study," *J. Therm. Anal. Calorim.*, vol. 123, no. 1, pp. 501–510, 2016.

- [47] J. M. Younker, A. Beste, and A. C. Buchanan III, "Computational Study of Bond Dissociation Enthalpies for Substituted ss-O-4 Lignin Model Compounds," *ChemPhysChem*, vol. 12, no. 18, pp. 3556–3565, 2011.
- [48] S. Kim *et al.*, "Computational study of bond dissociation enthalpies for a large range of native and modified Lignins," *J. Phys. Chem. Lett.*, vol. 2, no. 22, pp. 2846–2852, 2011.
- [49] P. C. A. Bruijninx and B. M. Weckhuysen, "Biomass conversion: Lignin up for break-down," *Nat. Chem.*, vol. 6, no. 12, pp. 1035–1036, 2014.
- [50] H. Wang, H. Wang, E. Kuhn, M. P. Tucker, and B. Yang, "Production of Jet Fuel-Range Hydrocarbons from Hydrodeoxygenation of Lignin over Super Lewis Acid Combined with Metal Catalysts," *ChemSusChem*, vol. 11, no. 1, pp. 285–291, 2018.
- [51] Y. Hu, G. Jiang, G. Xu, and X. Mu, "Hydrogenolysis of lignin model compounds into aromatics with bimetallic Ru-Ni supported onto nitrogen-doped activated carbon catalyst," *Mol. Catal.*, vol. 445, pp. 316–326, 2018.
- [52] L. Nie and D. E. Resasco, "Kinetics and mechanism of m-cresol hydrodeoxygenation on a Pt/SiO₂ catalyst," *J. Catal.*, vol. 317, pp. 22–29, 2014.
- [53] D. J. Rensel, S. Rouvimov, M. E. Gin, and J. C. Hicks, "Highly selective bimetallic FeMoP catalyst for C-O bond cleavage of aryl ethers," *J. Catal.*, vol. 305, pp. 256–263, 2013.
- [54] K. Lee, G. H. Gu, C. A. Mullen, A. A. Boateng, and D. G. Vlachos, "Guaiacol hydrodeoxygenation mechanism on Pt(111): Insights from density functional theory and linear free energy relations," *ChemSusChem*, vol. 8, no. 2, pp. 315–322, 2015.
- [55] P. T. M. Do, A. J. Foster, J. Chen, and R. F. Lobo, "Bimetallic effects in the hydrodeoxygenation of meta-cresol on γ -Al₂O₃ supported Pt–Ni and Pt–Co catalysts," *Green Chem.*, vol. 14, no. 5, p. 1388, 2012.
- [56] H. Wu, J. Song, C. Xie, C. Wu, C. Chen, and B. Han, "Efficient and Mild Transfer Hydrogenolytic Cleavage of Aromatic Ether Bonds in Lignin-Derived Compounds over Ru/C," *ACS Sustain. Chem. Eng.*, vol. 6, no. 3, pp. 2872–2877, 2018.
- [57] Q. Tan *et al.*, "Different Product Distributions and Mechanistic Aspects of the Hydrodeoxygenation of m-Cresol over Platinum and Ruthenium Catalysts," *ACS Catal.*, vol. 5, no. 11, pp. 6271–6283, 2015.
- [58] L. Zhang, K. Chen, B. Chen, J. L. White, and D. E. Resasco, "Factors that Determine Zeolite Stability in Hot Liquid Water," *J. Am. Chem. Soc.*, vol. 137, no. 36, pp. 11810–11819, 2015.

- [59] P. A. Zapata, J. Faria, M. P. Ruiz, R. E. Jentoft, and D. E. Resasco, "Hydrophobic zeolites for biofuel upgrading reactions at the liquid-liquid interface in water/oil emulsions," *J. Am. Chem. Soc.*, vol. 134, no. 20, pp. 8570–8578, 2012.
- [60] F. Anaya, L. Zhang, Q. Tan, and D. E. Resasco, "Tuning the acid-metal balance in Pd/ and Pt/zeolite catalysts for the hydroalkylation of m-cresol," *J. Catal.*, vol. 328, pp. 173–185, 2015.
- [61] D. M. Alonso *et al.*, "Increasing the revenue from lignocellulosic biomass: Maximizing feedstock utilization," *Sci. Adv.*, vol. 3, no. 5, 2017.
- [62] T. N. Pham, D. Shi, T. Sooknoi, and D. E. Resasco, "Aqueous-phase ketonization of acetic acid over Ru/TiO₂/carbon catalysts," *J. Catal.*, vol. 295, pp. 169–178, 2012.
- [63] T. N. Pham, D. Shi, and D. E. Resasco, "Kinetics and Mechanism of Ketonization of Acetic Acid on Ru/TiO₂ Catalyst," *Top. Catal.*, vol. 57, no. 6–9, pp. 706–714, 2013.
- [64] J. I. Di Cosimo, V. K. Díez, and C. R. Apesteguía, "Base catalysis for the synthesis of α,β -unsaturated ketones from the vapor-phase aldol condensation of acetone," *Appl. Catal. A Gen.*, vol. 137, no. 1, pp. 149–166, 1996.
- [65] W. T. Reichle, "Pulse microreactor examination of the vapor-phase aldol condensation of acetone," *J. Catal.*, vol. 63, no. 2, pp. 295–306, 1980.
- [66] J. I. Di Cosimo and C. R. Apesteguía, "Study of the catalyst deactivation in the base-catalyzed oligomerization of acetone," *J. Mol. Catal. A Chem.*, vol. 130, no. 1–2, pp. 177–185, 1998.
- [67] M. León *et al.*, "Consequences of MgO activation procedures on its catalytic performance for acetone self-condensation," *Appl. Catal. B Environ.*, vol. 147, pp. 796–804, 2014.
- [68] M. Kim, J. Park, H. P. R. Kannapu, and Y.-W. Suh, "Cross-Aldol Condensation of Acetone and n-Butanol into Aliphatic Ketones over Supported Cu Catalysts on Ceria-Zirconia," *Catalysts*, vol. 7, no. 9, p. 249, 2017.
- [69] L. Faba, E. Díaz, and S. Ordóñez, "Gas phase acetone self-condensation over unsupported and supported Mg-Zr mixed-oxides catalysts," *Appl. Catal. B Environ.*, vol. 142–143, pp. 387–395, 2013.
- [70] L. Faba, E. Díaz, and S. Ordóñez, "Improvement of the stability of basic mixed oxides used as catalysts for aldol condensation of bio-derived compounds by palladium addition," *Biomass and Bioenergy*, vol. 56, pp. 592–599, 2013.

- [71] J. T. Kozlowski and R. J. Davis, "Heterogeneous catalysts for the guerbet coupling of alcohols," *ACS Catal.*, vol. 3, no. 7, pp. 1588–1600, 2013.
- [72] N. N. Duong, "Stabilization of Pyrolysis Bio-oil Fractions for Refinery Insertion: Upgrading the Real Fractions and Model Compound Study," Univeristy of Oklahoma, 2014.

Appendix A. Effect of External Water on Acetone Aldol Condensation over MgO

A1 Introduction

Staged pyrolysis of biomass has been shown to be one of an important route to decompose biomass. A significant amount of carboxylic acids is obtained in the bio-oil. Extensive studies over the past decades have shown that ketonization is an effective method for acids upgrading to ketone and remove oxygen in the form of water and CO₂. This ketone is produced to a desirable building block that can undergo C-C coupling through aldol condensation. [3], [62], [63]

Vapor phase acetone aldol condensation have been studied in early 1960 by many researchers. It is well known that the results of the aldol condensation of acetone results in C₆-C₁₂ carbon that can undergo further deoxygenation to produce hydrocarbon from transportation fuels. Condensation of acetone is a typical base-catalyzed reaction. J.J. Di Cosimo et al. studied the vapor phase of self-condensation of acetone over MgO and alkaline metal additional to magnesium oxide. They observed that MgO is readily catalyzed the reaction and forms mesityl oxides and isophorone. When MgO was doped with alkaline or alkaline earth metal ions, the number of basic sites increases. Nevertheless, the activity of the catalyst increases proportionally to the surface basic sites concentration. This indicates that the rate-determining step is controlled by the surface basicity. [64]–[70]

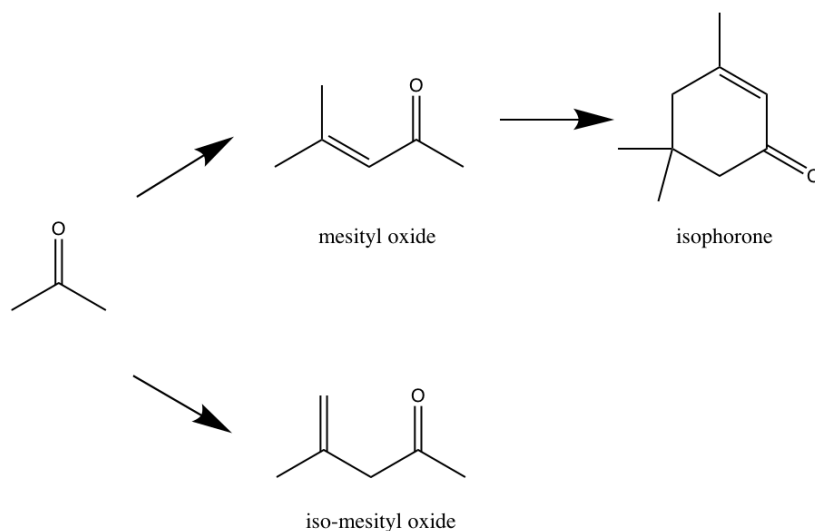


Figure A.1. Reaction pathway of acetone aldol condensation.

Not only that MgO is known for the aldol condensation, MgO has been studied vastly on Guerbet reaction. Guerbet reaction involves the coupling of two alcohol molecules such as ethanol to produce 1-butanol. The common pathway of this reaction consists of dehydrogenation of the alcohol to an aldehyde then a self-condensation to crotonaldehyde, followed by hydrogenation of the condensation product to 1-butanol. [71]

Previously in our group, MgO prepared by a combustion method, has been studied in both in self-condensation of cyclopentanone and cross-condensation of cyclopentanone and acetone in the liquid phase. Cyclopentanone is a representative intermediate cyclic ketone that resulted from the furanic compounds from pyrolysis of biomass that undergo a metal-catalyzed hydrogenation. The studies have shown that both of these aldol condensations suffered deactivation largely due to in situ water formation and over-condensates products accumulate on the surface of the catalyst. Such problem of in situ water accumulation has been overcome by functionalizing MgO with a hydrophobic

organosilane. The organosilane is believed to help remove the in situ water from the MgO surface.

Figure 5.2 indicates different trends in the rate of 2-cyclopentylidene-cyclopentanone formation for each MgO catalyst when increasing amounts of water are added. In MgO-NC, which is a combustion catalyst without functionalization, it shows a negative effect with the addition of water in the system from a sharp decrease in the rate. This implies that the water is presumably blocking the active site and inhibit the adsorption of the reactant. In contrast, the profile of MgO(70)-OTS(30) are divided into two regions with 0.355 mL of additional water being the turning point and the saturation point of water being vapors to start condensing as droplets. The rate of formation enhances to a factor of 2 from no water to saturation point then as the volume increases the rate decreases. Meanwhile, MgO(70)-ETS(30) exhibits a higher activity per gram than MgO(70)-OTS(30). This is largely due to the difference in lengths of the carbon chain on the silylating agents. With a shorter ethyl group in ETS, one should expect a lesser mass transfer limitation of the cyclopentanone molecules.

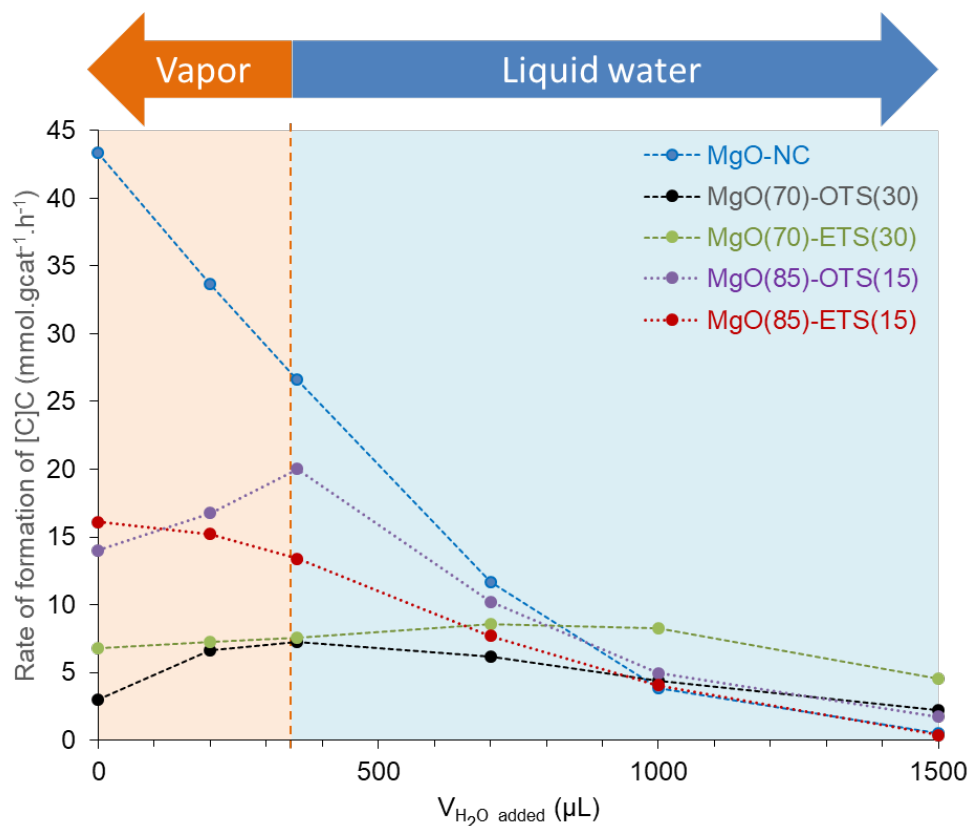


Figure A.2. Rate of formation of 2-cyclopentylidene-cyclopentanone over different volume of external water on different MgO catalysts in organic phase reaction from Duong Ngo’s research.

From the ascribing positive effect with the addition of water in the hydrophobic catalyst, the vapor phase aldol condensation over MgO catalysts was investigated. However, the catalytic conversion was studied over acetone to minimize the condensation of large dimer and trimer in the transfer line from the reactor to online GC-FID.

A2 Catalyst and Reaction Experiments

A2.1 Combusted MgO Preparation and Characterizations

MgO was prepared by thermal decomposition method using $Mg(NO_3)_2$ as a precursor. Firstly, $Mg(NO_3)_2$ was dissolved in deionized water until the solution became clear. Next, citric acid in a molar ratio of 1:2 mol acids to mol of Mg atom was slowly added. The

mixture was heated at 80°C for 1 hour while stirring to concentrate the solution on the hot plate. After that, the mixture was transferred and combusted inside a pre-heated 100°C oven. The oven was ramped to 550°C and held for 12 hours in air. The resulting material was grinded into a fine powder then sieved to 90 µm to 250 µm particles size.

A functionalized MgO catalyst was prepared by mixing toluene and the silylating agent in the ratio of 50 mL of toluene per gram of MgO. Octadecyltrichlorosilane (OTS) and ethyltrichlorosilane (ETS) were used to functionalize the surface of MgO. The suspension was stirred for 12 hours at 700 rpm at room temperature. The resulting catalyst was washed with excess methanol and dried for 12 hours at 110°C in the oven under static air to yield organosilane-functionalized MgO. MgO that had been modified with OTS was named MgO(x)-OTS(y) while MgO(x)-ETS(y) was abbreviated for the material had been functionalized with ETS. ‘x’ and ‘y’ are the theoretical wt.% of MgO and corresponding silylating agent respectively.

The BET surface area of all the catalysts was measured using N₂ physisorption on a Micromeritics ASAP 2010 instruments. The measurements were taken at liquid nitrogen temperature. Typically, 100 mg of samples were degassed at 200°C for 6 hours prior to the analysis.

A2.2 Reaction Experiments

Vapor phase aldol condensation of acetone was carried out in an isothermal tubular reactor. In each experiment, the catalyst was held at the center of a 6 mm-ID quartz tube between quartz wool. Inert glass beads were packed on top of the catalyst to top of the quartz tube for a well-dispersed flow of the reactants. A 60 mL/min of N₂ flow was passed

through for 1 hour at 250°C prior to the reaction to remove any adsorbed species. Acetone diluting in hexane in the volumetric ratio of 1:1 was fed continuously from a syringe pump and vaporized into the stream of N₂. The reactor was connected to the six-port sampling valve, heated to 250°C to avoid the condensation. The vapor stream was analyzed using Hewlett Packard 6890 GC-FID equipped with a Phenomenex ZB-Wax polyethylene glycol column (30 m x 0.25 mm x 0.25 μm). In case of addition of external water, 0.01 ml/hr of water was fed through a different syringe pump. In all the experiments, the carbon balance was kept above 90%.

A3 Results and Discussions

From the previous studied in our group, aldol condensation of cyclopentanone underwent self-aldol condensation and cross-aldol condensation with acetone to generate a pool of α,β -unsaturated ketones. The reaction was favorable in organic solvents in the liquid phase reaction at the temperature range of 150 – 200°C. Nevertheless, having a high surface area and a great number of active sites, the activity of MgO dropped tremendously after a few hours due to the formation of in situ water that is the by-product from aldol condensation and oligomers from the continuous condensation of intermediates that accumulate on the catalyst surface. To overcome such disadvantageous of the catalyst, the functionalization of an organosilane on MgO was proven to have a great improvement in the stability of the catalyst. The initial activity of the functionalized MgOs is less than that of the parent MgO but eventually, the functionalized MgOs would outperform. The functionalized catalyst had shown to resist to attack of the external water.

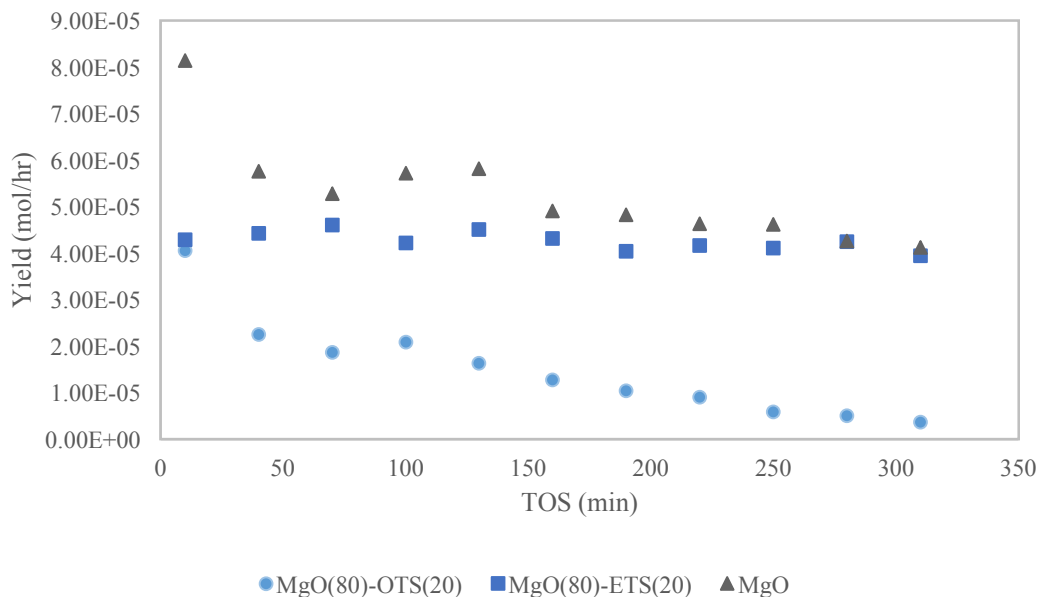


Figure A.3. Total yield of products over MgO, MgO(80)-OTS(20) and MgO(80)-ETS(20) at 250°C.

Figure 5.3 indicates that the trends in the total product yields in MgO and MgO(80)-OTS(20) were similar. In the case of MgO, after the initial period (10 min), there was a sharp decrease and after that, the total yield of the products slowly decreased. The activity of MgO started at two times higher than both the functionalized MgO. The initial period of both MgO(80)-OTS(20) and MgO(80)-ETS(20) started at the same level. MgO(80)-OTS(20) activity slowly dropped from its maximum at the initial over the time. The results of MgO and MgO(80)-OTS(20) confirms both of the catalysts experienced deactivation from *in situ* water formation and possibly large trimeric and oligomeric accumulated on their catalytic surface. MgO(80)-ETS(20) on the other hand displays a different scenario. As mentioned that the initial yield was similar to the OTS functionalized catalyst but the total yield of the products was a plateau and did not see any decreasing over 310 minutes of reaction. A vast difference between the results of the

two functionalized catalyst could be due to the difference in the alkyl chain length of the organosilane. When the organosilane group is introduced to MgO, the coverage of hydrophobic tails on active sites are influenced by the difference in alkyl chain length. The mass transfer limitation is one of the examples. When OTS is replaced with ETS, one would expect ETS to have less mass transfer limitation. Therefore, the catalytic activity with ETS functionalized MgO would expect to be higher than OTS catalyst.

The three products that were observed in acetone aldol condensation are mesityl oxide and its isomer so-called iso-mesityl oxide and also isophorone, an α,β -unsaturated cyclic ketone. The mechanism of the steps is shown in Figure 5.4 The first step of acetone aldol condensation is the abstraction of the proton in α -hydrogen, thereby forming an enolate. Then, the enolate attacks nearby ketone at electrophilic carbonyl carbon resulting an intermediate alkoxide. At this point, the alkoxide deprotonates a proton from the base leading to a β -hydroxy ketone. The ketone dehydrates rapidly to mesityl oxide. Subsequently, mesityl oxide could be attacked by an enolate on the surface form a 3-hydroxy-3,5,5-trimethylcyclohexan-1-one intermediate which consequently dehydrates to isophorone.

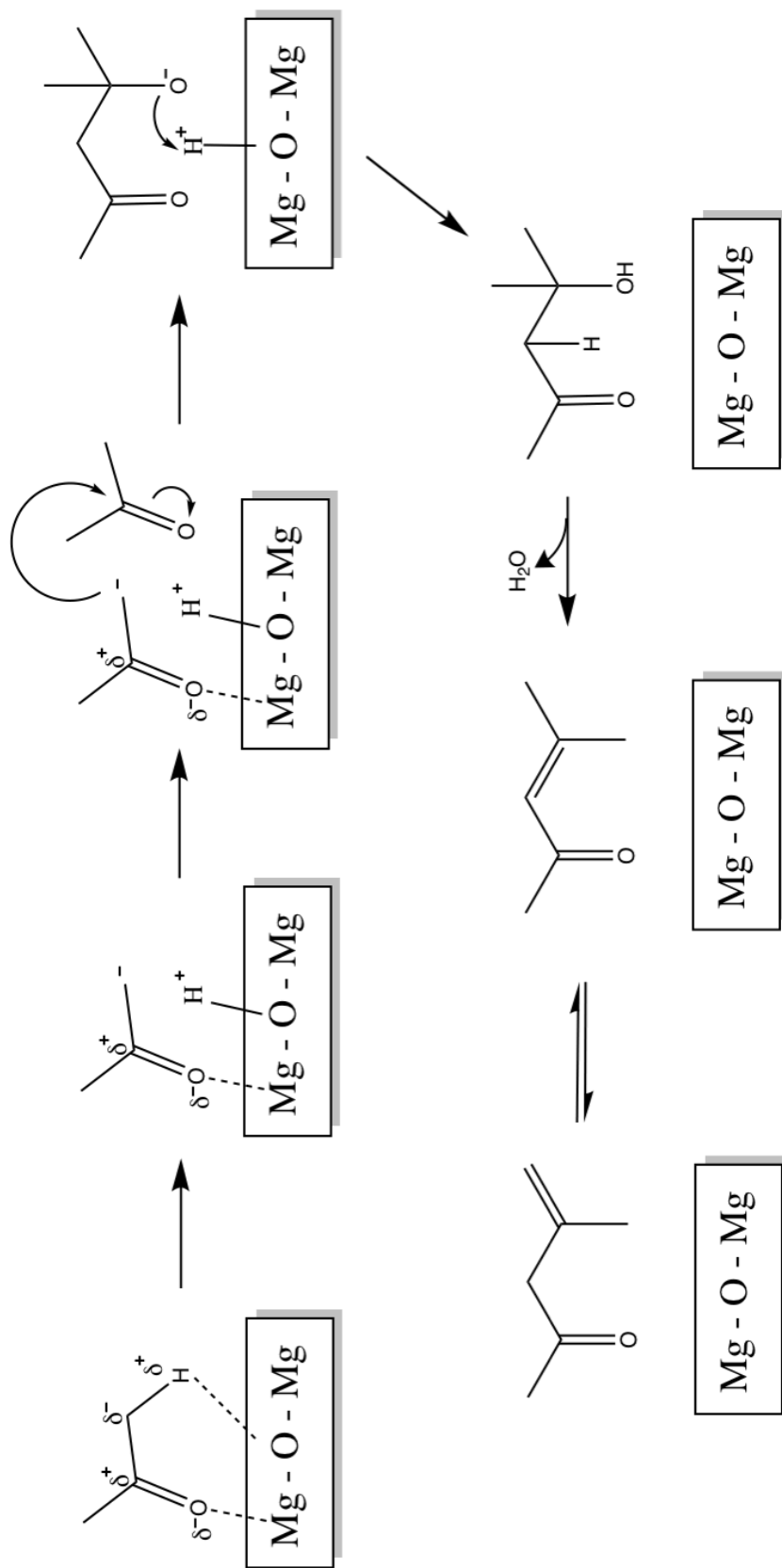


Figure A.4. Mechanism for mesityl oxide formation.

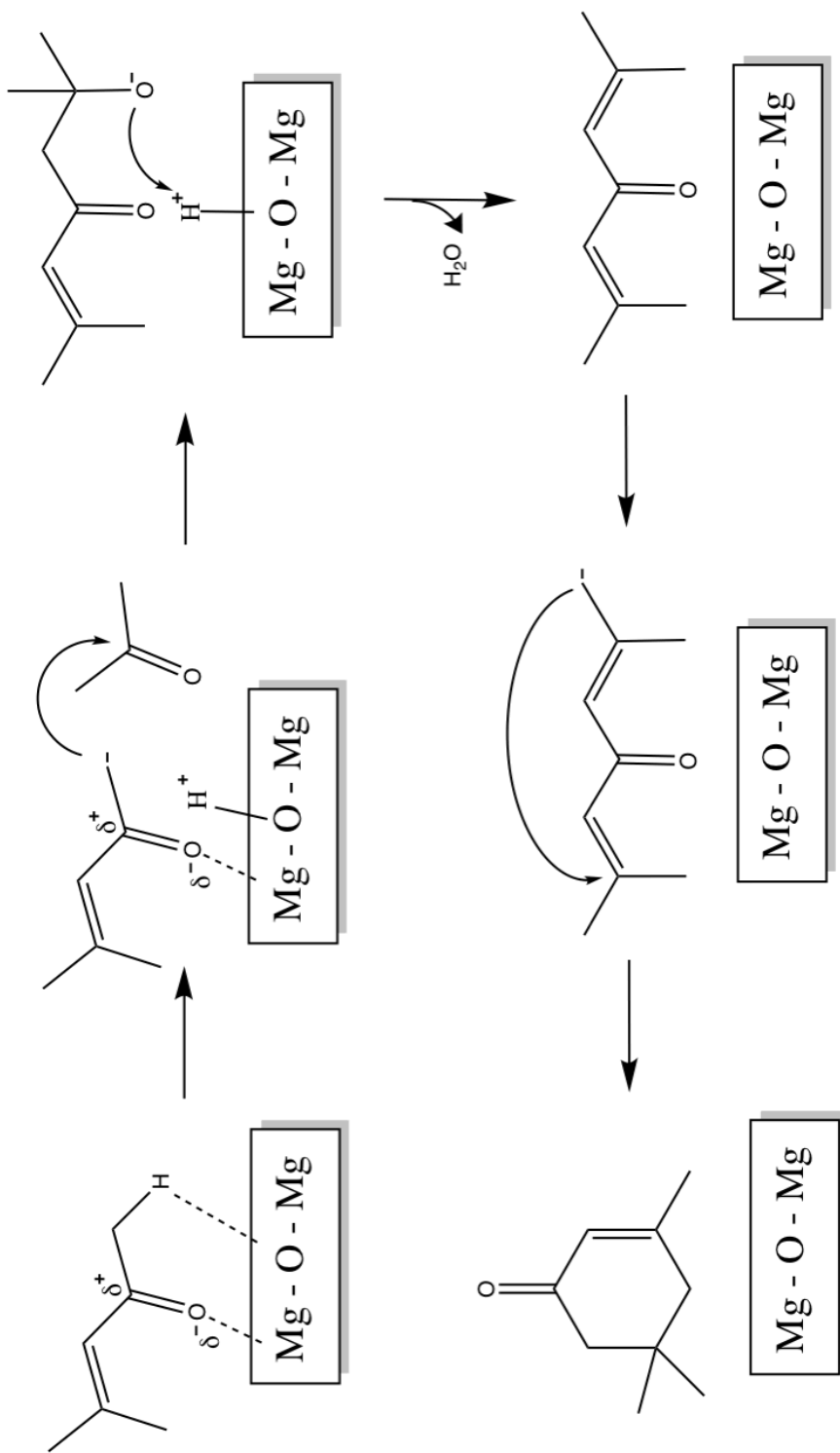


Figure A.5. Mechanism for isophorone formation.

While in liquid phase study, additional of external water, has shown the positive effect and considerably higher stability on functionalized MgO with respect to the regular MgO. In the vapor phase study, 0.01 ml/hr of external water was co-fed with acetone. The results are vastly different from that observed in the liquid phase. In all cases, the activity of the catalyst with an additional of external water tremulously decreased. The total yields depict that there was almost no activity in all the catalysts. This implies that the external water competitively adsorbed on the active sites and transform MgO into the inactive hydroxide, Mg(OH₂). Even though that this undesired adsorption could be inhibited by the hydrophobic catalyst but in this vapor phase study had shown otherwise.

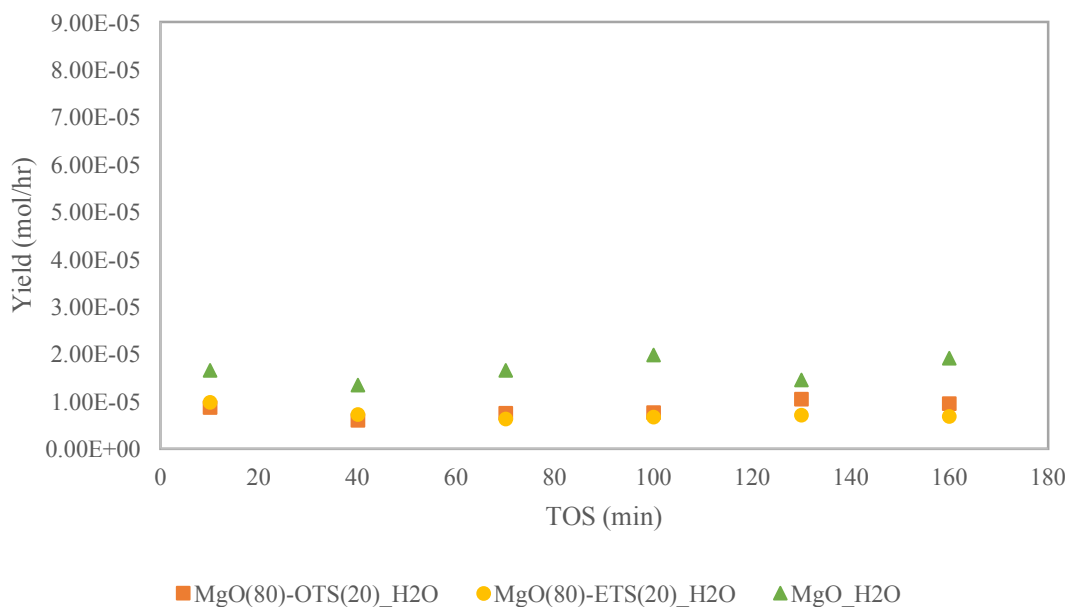


Figure A.6. Influence of addition of water on aldol condensation activity over MgO, MgO(80)-OTS(20) and MgO(80)-ETS(20) at 250°C.

A4 Conclusion

Influence of addition of water on aldol condensation of acetone was studied on combustion MgO and hydrophobic MgO. According to the liquid phase studies, both MgO-OTS and MgO-ETS have a positive effect on the activity of aldol condensation. However, in the vapor phase reaction, the addition of water shows otherwise in all cases. This could be a strong adsorption of water on the active sites that prohibit the adsorption of acetone.

Appendix B. Supplementary Figures and Tables

Table B.1. Effective Carbon Number (ECN) contributing to each compound groups from [72].

Compound Group	Effective Carbon no. Contribution
Aliphatic C	0.9845
Aromatic C	0.9416
C attached to aromatic ring	0.8442
Acid C	-0.3000
Carbonyl C	-0.0658
C_OH primary	0.4775
C_OH secondary	0.3979
C_OH tertiary	0.8796
C_OH phenolic	0.1165
ether C	0.2826
E ther C ring	-0.5202
Ester	-0.4585
ether to aromatic ring	-0.0191

Table B.2. Effective carbon number and respond factor for each monomers from lignin ethanolysis.

Compound	ECN	RF (area/g/mL)
2-methoxy,6-methyl phenol	5.3502	169888
phenol,3-ethyl	6.7933	243997
phenol,2,5-dimethyl	6.7931	243997
phenol,4-ethyl-2 methoxy	6.3346	182621
2,5-diethyl phenol	8.7620	255969
phenol,2-methoxy-4-propyl	7.3191	193207
phenol,2,6 dimethoxy	3.9072	111179
phenol,3(1,1-dimethylethyl)-4-methoxy	8.3035	202146
1,2,3-trimeoxybenzene	4.2738	111475
benzene,1,2,3-trimeoxy-5-methyl	5.2582	126603
1-(2,5-dimthoxyphenyl)-propanol	7.0991	158716

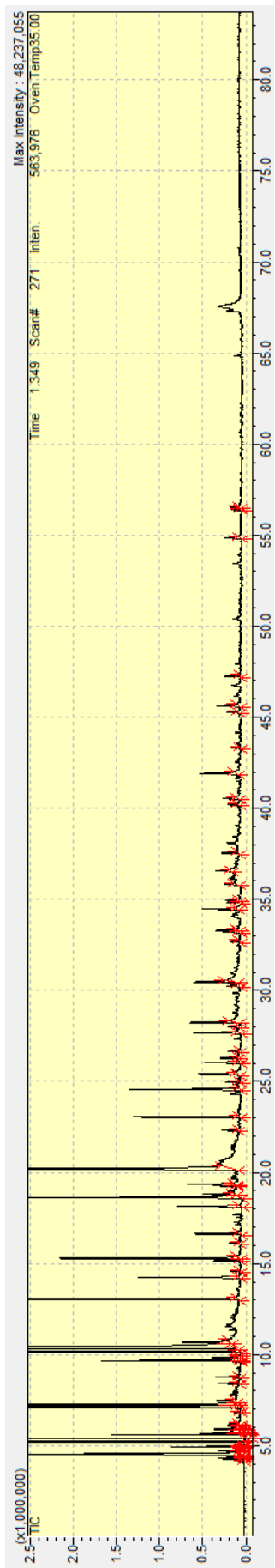


Figure B.1. Chromatogram of lignin ethanolsis.